

Electroweak Radiation in Antenna Parton Showers

Ronald Kleiss^a Rob Verheyen,^{a,b,1}

^a*Radboud University Nijmegen, 6500 GL Nijmegen, The Netherlands*

^b*University College London, WC1E 6BT London, United Kingdom*

E-mail: r.verheyen@ucl.ac.uk

ABSTRACT: We present the implementation of electroweak radiation in the Vincia parton shower. Due to the chiral nature of the electroweak theory, it is important to include explicit spin dependence in the shower algorithm. We thus use the spinor-helicity formalism to compute helicity-dependent branching kernels, taking special care to deal with the gauge relics that may appear in computation that involve longitudinal polarizations of the massive electroweak vector bosons. These kernels are used to construct a shower algorithm that includes all possible final-state electroweak branchings, including those induced by the Yang-Mills triple vector boson coupling and all Higgs couplings, as well as vector boson emissions from the initial state. We include a preliminary treatment of the effects of bosonic interference and the overlap between electroweak branchings and resonance decays, which are features that are exclusive to the electroweak theory. Some qualifying results on electroweak branching spectra at high energies, as well as effects on LHC physics are presented.

arXiv:2002.09248v1 [hep-ph] 21 Feb 2020

¹Corresponding author.

Contents

1	Introduction	1
2	The Spinor-Helicity Formalism	2
2.1	Spinors	2
2.2	Polarization Vectors	3
2.3	Spinor Products and Amplitude Evaluation	3
3	Electroweak Branching Amplitudes	4
4	Collinear Limits of the Branchings Amplitudes	9
5	The Electroweak Shower Implementation	12
5.1	Ordering and Resonance Showers	12
5.2	Recoiler Selection	14
5.3	Bosonic Interference	15
5.4	Overestimate Determination	17
5.5	Overview of the Shower Algorithm	19
6	Results	19
6.1	Branching Spectra	19
6.2	Bosonic Interference	22
6.3	Electroweak Corrections to Proton Collision Processes	23
7	Conclusion and Discussion	26
A	Relevant Feynman Rules of the Electroweak Theory	28
B	Branching amplitudes	29
B.1	Vector Boson Emission	30
B.1.1	Vector Boson Emission from Fermion	30
B.1.2	Vector Boson Emission from Antifermion	30
B.1.3	Vector Boson Emission from Vector Boson	31
B.2	Higgs Emission	32
B.2.1	Higgs Emission from Fermion	32
B.2.2	Higgs Emission from Antifermion	32
B.2.3	Higgs Emission from Vector Boson	32
B.2.4	Higgs Emission from Higgs	32
B.3	Vector Boson Splitting	32
B.3.1	Vector Boson Splitting to Fermion-antifermion	32
B.4	Higgs Splitting	33
B.4.1	Higgs Splitting to Fermion-antifermion	33

B.4.2	Higgs Splitting to Vector Bosons	33
B.5	Vector Boson Emission (Initial State)	34
B.5.1	Vector Boson Emission from Fermion	34
B.5.2	Vector Boson Emission from Antifermion	35

1 Introduction

Beyond the discovery of the Higgs boson [1, 2], signs of new physics have yet to appear at the LHC and the Standard Model has so far survived all forms of scrutiny. It has therefore become more likely that the Standard Model continues to describe nature accurately up to very high energy scales. At these very high energies heavy particles like electroweak gauge bosons, Higgs bosons and top quarks can start to appear as constituents of jets [3, 4] or otherwise contribute to radiative corrections. These types of electroweak radiative corrections have been shown to become sizeable even at LHC energies [5–18]. For instance, corrections to transverse momentum at LHC energies can already reach about 10% for exclusive dijet production [14, 15], and about 20% for single vector boson production [16–18], and they can be expected to grow even larger at future collider energies [19, 20]. Recently, ATLAS has reported on measurements that are sensitive to the collinear enhancements associated with W radiation in jets [21]. There, it is also pointed out that these types of effects will play a significant role for several measurements at high energy scales, which will become more abundant as the LHC gathers more data. It is therefore desirable to incorporate these electroweak effects in a systematic way in Monte Carlo simulations.

Electroweak corrections have been incorporated in parton showers in the past. An implementation [22, 23] is available in Pythia event generator [24] which only includes the radiation of electroweak gauge bosons and does not retain any spin information. The radiation of electroweak gauge bosons was similarly included in the Sherpa event generator [25] to study W emissions in jets [26]. Another approach [27] was employed in ALPGEN [28] where fixed-order matrix element calculations are combined with analytic Sudakov factors to achieve results similar to those of an electroweak parton shower. A more recent work [29] has implemented an electroweak shower in the Pythia 1 \rightarrow 2 transverse momentum ordered shower formalism that retains spin information and includes all branchings that may be found in the electroweak sector.

In this paper, we set up an electroweak parton shower based on the spinor-helicity formalism. It is implemented in the Vincia parton shower [30–32] which is a plugin to the Pythia event generator and already allows for QCD evolution with partons of definite helicity states [33, 34]. This feature is especially important in the electroweak theory due to its chiral nature. The electroweak shower described in this paper will thus be responsible for the electroweak component of the shower evolution, and is interleaved with the default Vincia QCD shower.

The shower formalism described here is based on a very different approach than that described in [29] and employs many different solutions for the subtleties involved in the

construction of an electroweak shower. In particular, it makes use of the spinor-helicity formalism to compute its branching kernels. The methods employed here are comparable with those used in [35, 36] to compute helicity-dependent QCD antenna functions. However, due to significant differences in the details of our procedure, we start with a brief overview of the spinor-helicity formalism and the conventions used in the calculation of the branching kernels. In section 3, the spinor-helicity formalism is used to compute branching kernels for all branching processes in the electroweak sector. Section 4 discusses the collinear limits of those branching kernels given in terms of Altarelli-Parisi splitting functions [37]. The results in that section are found to be in agreement with [29]. Section 5 details the implementation of an electroweak shower in the Vincia framework and treats a number of peculiarities exclusive to the electroweak sector such as the presence of bosonic interference and the matching to resonance decays. To show the significance of an electroweak shower, its effects are investigated in 6 for highly energetic particles, but also at LHC energies. We finally conclude in section 7, describing some missing features particular to the electroweak theory that may be included at a later stage.

2 The Spinor-Helicity Formalism

Due to the chiral nature of the electroweak theory, it is important to calculate electroweak branching kernels for individual spin states. We choose to perform these calculations using the spinor-helicity formalism using definitions similar to those described in [38]. This method enables us to compute branching kernels that describe the correct soft and collinear factorization of particle branchings without having to commit to a particular representation of the Dirac algebra or an explicit form of fermionic spinors. We first briefly summarize our conventions and techniques.

2.1 Spinors

Helicity spinors for massive fermions may be defined as

$$u_\lambda(p) = \frac{1}{\sqrt{2p \cdot k}}(\not{p} + m)u_{-\lambda}(k) \text{ and } v_\lambda(p) = \frac{1}{\sqrt{2p \cdot k}}(\not{p} - m)u_\lambda(k), \quad (2.1)$$

where λ is the fermion helicity and k is a lightlike reference vector that defines the meaning of the helicity of the fermion. Due to its massive nature, helicity is not a Lorentz-invariant quantity and does not coincide with the chirality of the fermion. The spin vector associated with the spinors defined in eq. (2.1) is

$$s_\lambda^\mu = \frac{\lambda}{m} \left(p^\mu - \frac{m^2}{p \cdot k} k^\mu \right). \quad (2.2)$$

We therefore choose the reference vector

$$k = (1, -\vec{e}), \quad (2.3)$$

where \vec{e} is a unit vector pointing in the direction of \vec{p} . With this choice, the massive helicity spinors retain the usual meaning of helicity as the projection of spin along the

direction of motion. This choice also clarifies the dependence on the current Lorentz frame. If a boost is applied, the momenta p and k will generally no longer align in the new frame, indicating that the spin vector defined in eq. (2.2) no longer points along the direction of motion.

2.2 Polarization Vectors

The polarization vectors for a massive vector boson with momentum p are defined as

$$\epsilon_{\pm}^{\mu}(p) = \pm \frac{1}{\sqrt{2}} \frac{1}{2p \cdot k} \bar{u}_{\mp}(k) \not{p} \gamma^{\mu} u_{\pm}(k) \text{ and } \epsilon_0^{\mu}(p) = \frac{1}{m} \left(p^{\mu} - 2 \frac{m^2}{2p \cdot k} k^{\mu} \right), \quad (2.4)$$

where k is again given by eq. (2.3). Here, $\epsilon_{\pm}^{\mu}(p)$ are the transverse polarizations and $\epsilon_0^{\mu}(p)$ is the purely longitudinal polarization which only exists for massive vector bosons.

2.3 Spinor Products and Amplitude Evaluation

Having expressed all massive spinors and polarization vectors in terms of massless spinors, amplitudes for particles with definite helicities can now be calculated very efficiently. We first define the spinor product

$$S_{\lambda}(k_a, k_b) \equiv \bar{u}_{\lambda}(k_a) u_{-\lambda}(k_b) \quad (2.5)$$

for lightlike (reference) vectors k_a and k_b , which obey

$$|S_{\lambda}(k_a, k_b)|^2 = 2k_a \cdot k_b. \quad (2.6)$$

Furthermore, by choosing a basis for the spinors, a possible representation of these spinor products is given by

$$S_{\lambda}(k_a, k_b) = (\lambda k_a^2 + i k_a^3) \sqrt{\frac{k_b^0 - k_b^1}{k_a^0 - k_a^1}} - (\lambda k_b^2 + i k_b^3) \sqrt{\frac{k_a^0 - k_a^1}{k_b^0 - k_b^1}}, \quad (2.7)$$

which is easily evaluated. Using the spinors and polarization vectors of the previous section, all amplitudes can be expressed in terms of these spinor products. The structures that may appear look like

$$S_{\lambda}(k_a, p_i, p_j, \dots, k_b) \equiv \bar{u}_{\lambda}(k_a) \not{p}_i \not{p}_j \dots u_{\pm\lambda}(k_b), \quad (2.8)$$

where p_i, p_j, \dots may be massive. These structures may be expressed in terms of the spinor products eq. (2.5) by defining

$$\hat{p}_i = p_i - \frac{p_i^2}{2p_i \cdot k_i} k_i, \quad (2.9)$$

which is explicitly massless. Eq. (2.8) may then be written as

$$S_{\lambda}(k_a, p_i, p_j, \dots, k_b) = S_{\lambda}(k_a, \hat{p}_i) S_{-\lambda}(\hat{p}_i, p_j, \dots, k_b). \quad (2.10)$$

This procedure is then repeated, the next time making p_j massless by subtracting $(p_j^2/2\hat{p}_i \cdot p_j)\hat{p}_i$, until the expression consists of only spinor products which can be directly evaluated using eq. (2.7).

3 Electroweak Branching Amplitudes

We now use the spinor-helicity formalism to compute branching amplitudes in the electroweak theory. We first recount the phase space regions where radiative amplitudes factorize into a non-radiative amplitude and a radiative correction. The momentum and helicity assignment for the amplitudes is given by

$$M_1 = \bullet \text{---} p_I, \lambda_I \qquad M_2 = \bullet \text{---} \begin{array}{l} p_i, \lambda_i \\ \text{---} \\ p_j, \lambda_j \end{array} \qquad (3.1)$$

In the quasi-collinear limit [39, 40], where

$$p_i \cdot p_j \approx m_i^2, m_j^2 \text{ and } E_i^2, E_j^2 \gg p_i \cdot p_j, \qquad (3.2)$$

the energy sharing variable z can be defined by

$$p_i = zp_I \text{ and } p_j = (1-z)p_I. \qquad (3.3)$$

In this limit, the matrix element factorizes as

$$|M_2|^2 \stackrel{\text{col.}}{=} \frac{1}{Q^2} P(\lambda_I, \lambda_i, \lambda_j, z) |M_1|^2, \qquad (3.4)$$

where $Q^2 = (p_i + p_j)^2 - m_I^2$ and $P(\lambda_I, \lambda_i, \lambda_j, z)$ is the helicity-dependent Altarelli-Parisi splitting kernel [37, 41, 42]. This definition of Q^2 foreshadows that it will later on assume the role of the ordering scale of the electroweak shower. On the other hand, in the soft limit, where

$$E_j \approx m_j \text{ and } E_i \gg E_j \qquad (3.5)$$

the amplitude exhibits the usual eikonal factorization

$$M_2 \stackrel{\text{soft}}{=} M_1 \times c \frac{2p_i \cdot \epsilon_{\lambda_j}}{Q^2} \delta_{\lambda_I \lambda_i}, \qquad (3.6)$$

where c is some spin-dependent coupling.

The electroweak branching kernels should reduce to the above soft and collinear limits eq. (3.4) and eq. (3.6) in their respective phase space regions eq. (3.2) and eq. (3.5). To compute them, we use the following procedure:

1. Write down an operator that creates a particle with definite helicity
2. Show that these operators indeed lead to polarized states in the radiative and non-radiative amplitudes given by eq. (3.1)
3. Compute the branching kernel from the ratio between the radiative and non-radiative amplitudes

$$B_{\lambda_I, \lambda_i, \lambda_j}(p_I, p_i, p_j) = \left| \begin{array}{l} \bullet \text{---} p_i, \lambda_i \\ \text{---} \\ p_j, \lambda_j \end{array} \right|^2 \bigg/ \left| \bullet \text{---} p_I, \lambda_I \right|^2. \qquad (3.7)$$

One major difference between the methods used in [35, 36] and our method are the definitions of the operators that create particles with states of definite helicity. These are represented by the black dots in eq. (3.1). We take their Feynman rules to be

$$\begin{aligned}
\bullet \xrightarrow{p, \lambda} \text{blob} &= u_{-\lambda}(k) \\
\bullet \xleftarrow{p, \lambda} \text{blob} &= \bar{u}_{-\lambda}(k) \\
\bullet \text{---} \text{blob} &= \bar{\epsilon}_{\lambda}^{\mu}(\hat{p}) \\
\bullet \text{---} \text{blob} &= 1.
\end{aligned} \tag{3.8}$$

where the grey blob represents the rest of the Feynman diagram and the vector

$$\hat{p} = p - \frac{p^2 - m^2}{2p \cdot k} k \tag{3.9}$$

is again introduced such that the momentum associated with the polarization vector is on shell. To discuss some of the subtleties encountered in the calculation of branching kernels in the electroweak theory, we proceed here with the calculation of the branching kernel of vector boson emission from a fermion. A full list of all electroweak branching amplitudes, to be defined later on, is given in Appendix B.

If the emitted vector boson is a photon, the branching kernel will be very similar to their helicity-dependent analogue for gluon emission from a quark [33, 34]. On the other hand, the vector boson may be a Z -boson, in which case the chiral nature of its coupling will be reflected in the branching kernel, or it may be a W -boson, in which case the flavour of the fermion also changes. We treat all types of vector boson emission at the same time, using the notation of the Feynman rules described in Appendix A.

We first compute the non-radiative amplitude in case the outgoing particle is a massive fermion. We observe that

$$\bar{u}_{\lambda_I}(p_I) u_{-\lambda'_I}(k_I) = \sqrt{2p_I \cdot k_I} \delta_{\lambda_I, \lambda'_I}, \tag{3.10}$$

and as such the Feynman rule given in eq. (3.8) does indeed create a state of definite helicity in the non-radiative amplitude. We can therefore choose the helicity in the operators to be λ_I in both the non-radiative and radiative amplitude. The non-radiative amplitude is then simply given by

$$\begin{aligned}
M_1^f &= \bullet \xrightarrow{p_I, \lambda_I} \text{blob} \\
&= \bar{u}_{\lambda_I}(p_I) u_{-\lambda_I}(k_I) = \sqrt{2p_I \cdot k_I}.
\end{aligned} \tag{3.11}$$

$$P(z) \propto \left(\text{Diagram 1} + \text{Diagram 2} \right)^2$$

Figure 1. Illustration of the cause of the appearance of unitarity-violating games in a naive calculation of the splitting functions.

The branching amplitude becomes

$$M^{f \rightarrow f'V}(\lambda_I, \lambda_i, 0) = \frac{A_L}{Q^2} \bar{u}_{\lambda_i}(k_i) (\not{p}_i - m_i) (v + a\gamma^5) \times \left(\not{p}_j - 2 \frac{m_j^2}{w_j^2} \not{k}_j \right) (\not{p}_{ij} - m_I) u_{\lambda_I}(k_{ij}). \quad (3.16)$$

At this point, a common problem related to longitudinal polarization in the electroweak theory appears. Eq. (3.16) contains a contribution of the form

$$\not{p}_i \not{p}_j \not{p}_{ij} = Q^2 \not{p}_i + m_I^2 \not{p}_i - m_i^2 \not{p}_{ij}. \quad (3.17)$$

The term proportional to Q^2 will cancel against the propagator, yielding a contribution that is not singular in the quasi-collinear or soft limit. To make matters worse, this term leads to unitarity-violation at high energies, indicating a pathology in the method. These unitarity-violating terms appear because the calculation of branching amplitudes is not gauge-invariant, as is illustrated in Figure 1. Vector boson emissions are not described by the single Feynman diagram we have considered so far. Other diagrams where the vector boson is emitted from either an internal line, or some other external line also contribute. A similar situation formally appears for the calculation of QCD or QED branching kernels. In those cases, the left-over terms originating from the gauge choice, or equivalently those from other diagrams, are no cause for concern. They are not singular in the soft and quasi-collinear phase space regions and thus do not contribute to the leading-log precision of the parton shower. Instead, the nonsingular terms may be used as parameters for uncertainty estimation [31].

In the electroweak theory, this behaviour is spoiled by the presence of longitudinal polarizations. The definition in eq. (2.4) reveals that the longitudinal polarization has two contributions, one that scales like $\mathcal{O}(E/m)$ and one that scales like $\mathcal{O}(m/E)$. The first term is a scalar piece that is a remainder of the Goldstone boson from the unbroken theory and may lead to unitarity violating behaviour, while the second term is a vector piece originating from the $SU(2)$ and $U(1)$ gauge bosons. Having chosen to use eq. (2.4) as polarization vectors and using the reference vector of eq. (2.3) we have fixed our gauge and ended up with a gauge-dependent branching amplitude.

We point out that this same issue is discussed in [29]. There, the issue is dealt with by choosing a particularly suitable gauge and invoking the Goldstone equivalence principle. This method ensures that the unitarity-violations are automatically isolated and no gauge

artifacts remain. As we have already fixed our gauge, this avenue is not open to us. Fortunately, due to the analytic nature of the spinor-helicity formalism, the problematic terms are very easy to identify and remove manually. We are reassured in our method by the knowledge that the terms in question have no factors of Q^2 in the denominator, meaning they *must* cancel to prevent unitarity violation. The remaining terms all have a factor of Q^2 in the denominator, and can therefore not cancel against any other diagram.

After removing the unitarity-violating terms, the amplitudes for longitudinal vector boson emission become

$$\begin{aligned}
M^{f \rightarrow f'V}(\lambda, \lambda, 0) &= 2 \frac{A_L}{Q^2} \left[S_{-\lambda}(k_i, (v - \lambda a)(m_I^2 p_i - m_i^2 p_{ij}) + (v + \lambda a)m_i m_I p_j, k_{ij}) \right. \\
&\quad \left. - 2 \frac{m_j^2}{w_j^2} \left((v - \lambda a) S_{-\lambda}(k_i, p_i, k_j, p_{ij}, k_{ij}) + (v + \lambda a) m_I m_i S_{-\lambda}(k_i, k_j, k_{ij}) \right) \right] \\
M^{f \rightarrow f'V}(\lambda, -\lambda, 0) &= 2 \frac{A_L}{Q^2} \left[m_i (v - \lambda a) S_{-\lambda}(k_i, p_j - 2 \frac{m_j^2}{w_j^2} k_j, p_{ij}, k_{ij}) \right. \\
&\quad \left. + m_I (v + \lambda a) S_{-\lambda}(k_i, p_i, p_j - 2 \frac{m_j^2}{w_j^2} k_j, k_{ij}) \right]. \tag{3.18}
\end{aligned}$$

A full list of branching amplitudes as implemented in the electroweak shower is given in Appendix B. Vector boson radiation from the initial state is also included, for which the branching amplitudes may either be computed separately, or they may be obtained through crossing symmetry.

We point out that the formalism for the calculation of branching amplitudes described above may be extended to incorporate soft interference effects. In QCD showers, which function in the leading-colour approximation, these interference effects can be approximately incorporated by angular ordering [43], or they can be accounted for automatically when the branching kernels are dipoles [44, 45], antennae functions [31, 32, 46], or otherwise include soft corrections in the purely collinear Altarelli-Parisi splitting kernels [47]. An algorithm that includes the full multipole structure of QED radiation in the Vincia shower was described in [48, 49] which makes use of a single branching kernel that includes the full soft structure. Such kernels may also be computed using the above formalism. The Feynman rules defined in eq. (3.8) can be applied multiplicatively to create states of multiple particles with definite spin. An example may be written diagrammatically as

$$B_{\text{soft}} = \frac{\left| \begin{array}{c} \text{Diagram 1} \\ + \\ \text{Diagram 2} \\ + \\ \text{Diagram 3} \end{array} \right|^2}{\left| \begin{array}{c} \text{Diagram 4} \end{array} \right|^2}. \tag{3.19}$$

Since the amplitudes individually adhere to the correct soft limit, this branching kernel includes the complete multipole structure. The collinear limits are simultaneously included correctly, since a single diagram becomes dominant in its respective collinear limit. In [49] it was shown that the effects of soft interference are typically small and restricted to

very particular phase space regions. As such, the current Vincia implementation does not incorporate soft interference in the electroweak sector.

4 Collinear Limits of the Branchings Amplitudes

In this section we discuss the behaviour of the branching amplitudes in the quasi-collinear limit described by eq. (3.2). The reference vectors simplify to

$$k_i \stackrel{\text{col.}}{=} k_j \stackrel{\text{col.}}{=} k_{ij} \equiv k. \quad (4.1)$$

The branching amplitudes can be expressed in terms of the energy sharing variable z by replacing

$$p_i \rightarrow z p_{ij} \text{ and } p_j \rightarrow (1 - z) p_{ij}. \quad (4.2)$$

The only two remaining spinor products in the branching amplitudes are related by

$$S_{-\lambda}(k, p_j, p_i, k) = -S_{-\lambda}(k, p_i, p_j, k). \quad (4.3)$$

Up to a phase factor, they are

$$\begin{aligned} S_{-\lambda}(k, p_i, p_j, k) &\propto 2 \sqrt{p_i \cdot k_i p_j \cdot k_j} \sqrt{Q^2 + m_I^2 - m_i^2 \frac{p_{ij} \cdot k_{ij}}{p_i \cdot k_i} - m_j^2 \frac{p_{ij} \cdot k_{ij}}{p_j \cdot k_j}} \\ &\stackrel{\text{col.}}{=} 2 p_{ij} \cdot k \sqrt{z(1-z)} \sqrt{\tilde{Q}^2} \end{aligned} \quad (4.4)$$

where

$$\tilde{Q}^2 = Q^2 + m_I^2 - \frac{m_j^2}{1-z} - \frac{m_i^2}{z}. \quad (4.5)$$

Tables 1-4 contain the collinear limits of all electroweak branching amplitudes. These limits are related to the Altarelli-Parisi splitting kernels by

$$|M|^2 = \frac{1}{Q^2} P(z), \quad (4.6)$$

where M is the branching amplitude. For the sake of notation, the collinear limits are given using eq. (4.4) and are only correct up to a phase factor. Note that this phase factor is irrelevant for the calculation of the splitting kernels. The splitting functions found here agree with the results of [29].

We briefly discuss some similarities and differences between the electroweak splitting functions and those normally encountered in QCD for vector boson emission from a fermion. Considering the amplitudes in table 1, the first two splitting kernels correspond to a fermion emitting a transversely polarized vector boson and maintaining its helicity. These kernels display the standard spin-summed behaviour

$$P_{f \rightarrow f'V} \propto \frac{1+z^2}{1-z}, \quad (4.7)$$

as would be expected from the unbroken phase of the standard model where the vector bosons are massless and do not have a longitudinal polarization. Up to the coupling constant, the splitting function is identical to those for gluon emission from a fermion. The

λ_I	λ_i	λ_j	$f \rightarrow f'V \times \frac{1}{Q^2}$ and $\bar{f} \rightarrow \bar{f}'V \times \frac{1}{Q^2}$
λ	λ	λ	$\sqrt{2}\lambda(v - \lambda a)\sqrt{\tilde{Q}^2}\frac{1}{\sqrt{1-z}}$
λ	λ	$-\lambda$	$\sqrt{2}\lambda(v - \lambda a)\sqrt{\tilde{Q}^2}\frac{z}{\sqrt{1-z}}$
λ	$-\lambda$	λ	$\sqrt{2}\lambda\left[m_I(v - \lambda a)\sqrt{z} - m_i(v + \lambda a)\frac{1}{\sqrt{z}}\right]$
λ	$-\lambda$	$-\lambda$	0
λ	λ	0	$(v - \lambda a)\left[\frac{m_I^2}{m_j}\sqrt{z} - \frac{m_i^2}{m_j}\frac{1}{\sqrt{z}} - 2m_j\frac{\sqrt{z}}{1-z}\right] + (v + \lambda a)\frac{m_i m_I}{m_j}\frac{1-z}{\sqrt{z}}$
λ	$-\lambda$	0	$\sqrt{\tilde{Q}^2}\sqrt{1-z}\left[\frac{m_i}{m_j}(v - \lambda a) - \frac{m_I}{m_j}(v + \lambda a)\right]$

Table 1. Table of branching amplitudes for vector boson emission off a fermion for all helicity configurations. For the antifermion, the interchange $(v - \lambda a) \leftrightarrow (v + \lambda a)$ is applied.

λ_I	λ_i	λ_j	$V \rightarrow f\bar{f}' \times \frac{1}{Q^2}$
λ	λ	$-\lambda$	$\sqrt{2}\lambda(v - \lambda a)\sqrt{\tilde{Q}^2}z$
λ	$-\lambda$	λ	$\sqrt{2}\lambda(v + \lambda a)\sqrt{\tilde{Q}^2}(1-z)$
λ	λ	λ	$\sqrt{2}\lambda\left[m_i(v + \lambda a)\sqrt{\frac{1-z}{z}} + m_j(v - \lambda a)\sqrt{\frac{z}{1-z}}\right]$
λ	$-\lambda$	$-\lambda$	0
0	λ	λ	$\sqrt{\tilde{Q}^2}\left[\frac{m_i}{m_I}(v + \lambda a) + \frac{m_j}{m_I}(v - \lambda a)\right]$
0	λ	$-\lambda$	$(v - \lambda a)\left[2m_I\sqrt{z(1-z)} - \frac{m_i^2}{m_I}\sqrt{\frac{1-z}{z}} - \frac{m_j^2}{m_I}\sqrt{\frac{z}{1-z}}\right] + (v + \lambda a)\frac{m_i m_j}{m_I}\frac{1}{\sqrt{z(1-z)}}$

Table 2. Table of branching amplitudes for vector boson splitting to fermions for all helicity configurations.

presence of general particle masses induces a shift of $1/Q^2 \rightarrow \tilde{Q}^2/(Q^2)^2$. The fermionic mass corrections in \tilde{Q}^2 also appear for gluon emission and reproduce the mass contributions to the eikonal factor in the soft limit. For W and Z emission, a vector boson mass correction is also present.

The following two amplitudes describe transverse vector boson emission with a fermionic spin flip. The nonzero amplitude is mass-suppressed with respect to the previous amplitudes, meaning it only contributes significantly for values of $Q^2 \approx m_i^2, m_I^2$. These amplitudes also exist for photon and gluon emission off massive fermions, but here the flavour-changing property of W -emissions means that two separate mass terms of the pre-branching and post-branching fermions appear.

The very last amplitude describes longitudinal vector boson emission with a fermionic spin flip. In the unbroken phase of the Standard Model, the equivalent process is the emission of the corresponding Goldstone boson. The scalar splitting function

$$P_{f \rightarrow f\varphi} \propto (1-z) \quad (4.8)$$

is indeed recovered and the proportionality factor corresponds to the coupling to the Gold-

λ_I	λ_i	λ_j	$V \rightarrow V'V'' \times \frac{g_{VV'V''}}{Q^2}$	λ_I	λ_i	$(f \rightarrow fh \text{ and } \bar{f} \rightarrow \bar{f}h) \times \frac{1}{Q^2} \frac{e}{2s_w} \frac{m_f}{m_w}$
λ	λ	λ	$\sqrt{2}\lambda\sqrt{\tilde{Q}^2}\sqrt{\frac{1}{z(1-z)}}$	λ	λ	$m_f\left[\sqrt{z} + \frac{1}{\sqrt{z}}\right]$
λ	λ	$-\lambda$	$\sqrt{2}\lambda\sqrt{\tilde{Q}^2}z\sqrt{\frac{z}{1-z}}$	λ	$-\lambda$	$\sqrt{1-z}\sqrt{\tilde{Q}^2}$
λ	$-\lambda$	λ	$\sqrt{2}\lambda\sqrt{\tilde{Q}^2}(1-z)\sqrt{\frac{1-z}{z}}$	λ_i	λ_j	$h \rightarrow f\bar{f} \times \frac{1}{Q^2} \frac{e}{2s_w} \frac{m_f}{m_w}$
λ	$-\lambda$	$-\lambda$	0	λ	λ	$\sqrt{\tilde{Q}^2}$
0	λ	λ	0	λ	$-\lambda$	$m_f\left[\sqrt{\frac{1-z}{z}} - \sqrt{\frac{z}{1-z}}\right]$
0	λ	$-\lambda$	$m_I(2z-1) + \frac{m_j^2}{m_I} - \frac{m_i^2}{m_I}$			
λ	0	λ	$m_i\left(1 + 2\frac{1-z}{z}\right) + \frac{m_j^2}{m_i} - \frac{m_I^2}{m_i}$			
λ	0	$-\lambda$	0			
λ	λ	0	$m_j\left(1 + 2\frac{z}{1-z}\right) + \frac{m_i^2}{m_j} - \frac{m_I^2}{m_j}$			
λ	$-\lambda$	0	0			
λ	0	0	$\frac{\lambda}{\sqrt{2}} \frac{m_i^2+m_j^2-m_I^2}{m_i m_j} \sqrt{\tilde{Q}^2} \sqrt{z(1-z)}$			
0	λ	0	$\frac{\lambda}{\sqrt{2}} \frac{m_i^2+m_j^2-m_I^2}{m_I m_j} \sqrt{\tilde{Q}^2} \sqrt{\frac{1-z}{z}}$			
0	0	λ	$\frac{\lambda}{\sqrt{2}} \frac{m_i^2+m_j^2-m_I^2}{m_I m_i} \sqrt{\tilde{Q}^2} \sqrt{\frac{z}{1-z}}$			
0	0	0	$\frac{1}{2} \frac{m_I^3}{m_i m_j} (2z-1) - \frac{m_i^3}{m_I m_j} \left(\frac{1}{2} + \frac{1-z}{z}\right) + \frac{m_j^3}{m_I m_i} \left(\frac{1}{2} + \frac{z}{1-z}\right)$ $+ \frac{m_i m_j}{m_I} \left(\frac{1-z}{z} - \frac{z}{1-z}\right) + \frac{m_I m_i}{m_j} (1-z) \left(2 + \frac{1-z}{z}\right) - \frac{m_I m_j}{m_i} z \left(2 + \frac{z}{1-z}\right)$			

Table 3. Table of branching amplitudes for vector boson emission off a vector boson and all Higgs-fermion branchings for all helicity configurations. Since the Higgs is blind to fermion helicity, the amplitudes are identical for the fermion and the antifermion.

λ_I	λ_i	$V \rightarrow Vh \times \frac{g_{hVV}}{Q^2}$	λ_i	λ_i	$h \rightarrow VV \times \frac{g_{hVV}}{Q^2}$
λ	λ	-1	λ	λ	0
λ	$-\lambda$	0	λ	$-\lambda$	-1
0	λ	$\frac{1}{m_I} \frac{\lambda}{\sqrt{2}} \sqrt{\tilde{Q}^2} \sqrt{z(1-z)}$	0	λ	$\frac{1}{m_i} \frac{\lambda}{\sqrt{2}} \sqrt{\tilde{Q}^2} \sqrt{\frac{1-z}{z}}$
λ	0	$\frac{1}{m_i} \frac{\lambda}{\sqrt{2}} \sqrt{\tilde{Q}^2} \sqrt{\frac{1-z}{z}}$	λ	0	$\frac{1}{m_j} \frac{\lambda}{\sqrt{2}} \sqrt{\tilde{Q}^2} \sqrt{\frac{z}{1-z}}$
0	0	$\frac{1}{2} \frac{m_j^2}{m_i^2} + \frac{1-z}{z} + z$	0	0	$\frac{1}{2} \frac{m_I^2}{m_i^2} - 1 - \frac{1-z}{z} - \frac{z}{1-z}$

Table 4. Table of branching amplitudes for Higgs emission off vector bosons and Higgs splitting to vector bosons for all helicity configurations.

stone boson. The amplitude for longitudinal vector boson emission without spin flip is again mass-suppressed with respect to the spin flip case, which is the 'natural' mode of scalar emission. In contrast to the spin flip case, where only the scalar part of the longitudinal polarization survives, here a contribution from the vector piece proportional to the vector boson mass appears as well.

5 The Electroweak Shower Implementation

The electroweak shower is implemented in the Vincia framework, which was set out in [30–34, 50–52]. Here we first provide a brief summary before continuing with a description of some details specific to the electroweak shower.

Parton showers are constructed as a Markov chain of emissions that are distributed according to an approximation to the radiative matrix element. In the case of Vincia, such emissions are kinematically described as $2 \rightarrow 3$ branchings. As an example, in case both partons are part of the final state, the branching momenta are indicated as $I, K \rightarrow i, j, k$. The parton shower approximation is

$$|M_{n+1}|^2 d\Phi_{n+1} = |M_n|^2 d\Phi_n \times a(s_{ij}, s_{jk}) d\Phi_{\text{ant}}, \quad (5.1)$$

where

$$d\Phi_{\text{ant}}^{\text{FF}} = \frac{1}{16\pi^2} m_{IK}^2 \lambda^{-\frac{1}{2}}(m_{IK}^2, m_I^2, m_K^2) ds_{ij} ds_{jk} \frac{d\varphi}{2\pi}, \quad (5.2)$$

where $s_{ij} = 2p_i \cdot p_j$ and λ is the Källén function. Eq. (5.13) represents an exact factorization of the radiative phase space. An associated kinematic map is defined between the pre-branching and post-branching momenta that conserves total momentum and is soft- and collinear-safe [50]. The branching kernels are antenna functions $a(s_{ij}, s_{jk})$ that capture the leading collinear and soft singularities associated with QCD emissions. The equivalent expressions to eq. (5.1) for radiation from the initial state, as well as the definition of the kinematic maps, may be found in [51].

Vincia also supports QCD evolution of partons with definite helicity [33, 34], making for a natural framework for the inclusion of an electroweak shower. Interference effects between intermediate spin configurations have previously been incorporated in parton showers, such as in the Herwig [53, 54] parton shower [55] and in Deductor [56, 57]. The Vincia parton shower currently makes no attempt to incorporate spin interferences. Correspondingly, the same is true for the electroweak shower.

Note that Vincia, like all other parton showers currently function in the leading colour limit, although recently work has attempted to improve upon that [58–61]. In this limit, the soft interferences associated with gluon emissions span only between colour-adjacent partons, and as such they may be captured entirely in 3-parton antenna functions. The electroweak shower currently does not attempt to incorporate soft interference effects, and as such the branching kernels discussed above are only functions of i and j , while k functions as a kinematically-required recoiler.

5.1 Ordering and Resonance Showers

The electroweak shower includes a number of branchings that would normally be associated with the decay of resonances by Pythia [62]. In particular, the Standard Model particles that have such decay-like branchings are Z , W^\pm , Higgs and top quark. In Pythia, the scale of a resonance decay is always associated with the width of the resonance, as that characterizes its degree of off-shellness. With the inclusion of an electroweak shower, the decay modes of

the resonances are now also all present as shower branchings. The shower enables highly-energetic resonances to branch and disappear at scales much higher than their width, where they should indeed be treated as any other non-resonant particle. At scales close to the resonance width, the Breit-Wigner character of the resonance decay, which also involves a kind of resummation, should instead dominate the distribution. As such, the matching between the parton shower and the Breit-Wigner is not a straightforward issue, and will be the topic of an upcoming work [63]. Here, we instead choose to match the parton shower to a Breit-Wigner distribution smoothly through a simple sampling procedure.

To that end, we first define a suitable ordering scale. Branchings with large ordering scales should correspond to particles that are very far off-shell and are very short-lived. Resonance branchings come with the feature that regions of phase space with $Q^2 < 0$ appear. These kinds of branchings should be considered to be off-shell, and the ordering scale should be large for very negative values of Q^2 . As such, we define the ordering variable for all final-state branchings in the electroweak shower to be

$$|Q^2| = |(p_i + p_j)^2 - m_l^2|. \quad (5.3)$$

In the case of a resonance branching, this ordering scale approaches the Breit-Wigner peak from both sides. For all other types of branchings, Q^2 is strictly positive and the ordering scale corresponds to virtuality ordering, which regulates the soft-collinear and collinear singularities as required. For most types of non-resonant electroweak branchings the phase space is naturally cut off due to the masses of the post-branching momenta. Beyond resonance branchings, photon emission is the only remaining branching that is not cut off naturally. They are instead cut off at the same scale as the QCD shower, and QED radiation at lower scales is included as is described in [49].

We incorporate the Breit-Wigner shape by defining branching kernels $B_\Gamma(Q^2)$ through the replacement

$$\frac{1}{(Q^2)^2} \rightarrow \frac{1}{(Q^2)^2 + m^2\Gamma^2}, \quad (5.4)$$

where the width is currently taken to be fixed and we have dropped the other arguments of the branching kernel B for readability. One straightforward way to match the shower to this modified branching kernel is to define a fixed matching scale $|Q_{\text{match}}^2|$, leading to the distribution

$$\begin{aligned} S(Q_{\text{Start}}^2, Q^2) = & \theta(|Q_{\text{Start}}^2| > |Q^2| > |Q_{\text{Match}}^2|) B(Q^2) \Delta(|Q_{\text{Start}}^2|, |Q^2|) \\ & + \theta(|Q_{\text{Match}}^2| > |Q^2|) \Delta(|Q_{\text{Start}}^2|, |Q_{\text{Match}}^2|) \frac{B_\Gamma(Q^2)}{N(|Q_{\text{Match}}^2|)}, \end{aligned} \quad (5.5)$$

where θ is a step function that equals one if the condition inside the brackets is met, and zero otherwise. The function Δ is the usual Sudakov factor generated by the shower, using the unmodified branching kernels. Note that its arguments are absolute values of ordering scales since they concern the evolution between scales, while the branching kernels may depend on the sign of Q^2 . The Sudakov factor in the second term is the no-branching probability of the parton shower between the starting scale and the matching scale. It is a

constant that, together with the Breit-Wigner normalization $N(|Q_{\text{Match}}^2|)$ ensures that the total distribution is normalized.

The distribution given by eq. (5.5) is however not necessarily continuous or smooth. One may fix the continuity constraint by finding an adequate matching scale, but this may still not lead to a smooth distribution. A more general approach is to sample the matching scale from some probability distribution $\mathcal{P}(|Q_{\text{Match}}^2|)$ such that the branching distribution becomes

$$\begin{aligned} \tilde{S}(Q_{\text{Start}}^2, Q^2) = & B_0(Q^2) \Delta(|Q_{\text{Start}}^2|, |Q^2|) \int_0^{|Q^2|} d|Q_{\text{Match}}^2| \mathcal{P}(|Q_{\text{Match}}^2|) \\ & + \int_{|Q^2|}^{|Q_{\text{Start}}^2|} d|Q_{\text{Match}}^2| \mathcal{P}(|Q_{\text{Match}}^2|) \Delta(|Q_{\text{Start}}^2|, |Q_{\text{Match}}^2|) \frac{B_\Gamma(Q^2)}{N(|Q_{\text{Match}}^2|)}. \end{aligned} \quad (5.6)$$

The probability distribution $\mathcal{P}(|Q_{\text{Match}}^2|)$ may now be selected to yield a suitable function in the shower term. We make the choice

$$\int_0^{|Q^2|} d|Q_{\text{Match}}^2| \mathcal{P}(|Q_{\text{Match}}^2|) = \frac{(Q^2)^2}{(Q^2)^2 + m^2\Gamma^2}, \quad (5.7)$$

which leads to

$$\mathcal{P}(|Q_{\text{Match}}^2|) = \frac{1}{N_{\mathcal{P}}(|Q_{\text{Match}}^2|)} \frac{m^2\Gamma^2|Q_{\text{Match}}^2|}{((Q_{\text{Match}}^2)^2 + m^2\Gamma^2)^2}. \quad (5.8)$$

The choice of eq. (5.8) ensures that the probability distribution of eq. (5.6) is dominated by the parton shower contribution at high scales, while the Breit-Wigner contribution dominates at low scales.

The implementation within the parton shower framework is relatively straightforward. When a shower of a resonance is initiated, a matching scale $|Q_{\text{Match}}^2|$ is sampled from eq. (5.8), which serves as the cutoff scale. If during showering the branching scale drops below the matching scale, a new scale is instead drawn from the Breit-Wigner distribution through rejection sampling. This scale may still be allowed to compete against other shower branchings, and the usual parton shower kinematic maps are used to perform the decay kinematics.

We emphasize that this solution only serves as an approximate means of matching the shower to a Breit-Wigner, and a more sophisticated method that closely matches that of Pythia will be developed in [63].

5.2 Recoiler Selection

While in the QCD portion of a parton shower the colour structure dictates the pairings of partons I and K that branch, no such guidance exists in the electroweak sector. Furthermore, the branching kernels only describe the soft-collinear and collinear singularities associated with the branching of particle I , and as such the choice of pairing with a recoiler K is only relevant kinematically. The choice for K may be made probabilistically to minimize the physical consequences of the recoil on previously generated branchings. For the branching of particle i , the probability to select a spectator j from a pool of N available

ones is

$$\mathcal{P}_j = \frac{|M^{x \rightarrow ij}|^2}{\sum_{j=1}^N |M^{x \rightarrow ij}|^2}. \quad (5.9)$$

That is, for all N available spectators we check if the pair of particles i, j could have been created by the electroweak shower as a branching of particle x . All of the contributions in the denominator of eq. (5.9) thus correspond with possible shower histories that contribute to the current state. The selection of a spectator is then more likely if the shower history where the current brancher and that spectator were created by a previous branching. To clarify this further in terms of diagrams, an example is

$$\begin{aligned} \left| \text{Diagram} \right|^2 &= \frac{\left| \text{Diagram 1} \right|^2}{\left| \text{Diagram 1} \right|^2 + \left| \text{Diagram 2} \right|^2} \left| \text{Diagram 3} \right|^2 \\ &+ \frac{\left| \text{Diagram 4} \right|^2}{\left| \text{Diagram 1} \right|^2 + \left| \text{Diagram 2} \right|^2} \left| \text{Diagram 5} \right|^2. \end{aligned} \quad (5.10)$$

The spectator for the splitting of the vector boson is chosen to be either of the other external legs based on the probabilities that the vector boson was emitted by either of those legs. When the vector boson splits, it is brought off its mass shell by transferring some momentum of the spectator to the vector boson. Because the vector boson momentum is modified, the emission kernel that it was produced with is no longer completely correct. In the strong-ordering phase space region where $Q_{\text{emit}}^2 \gg Q_{\text{split}}^2$, relevant for the leading log contribution, this type of mismodelling is formally absent. However, to cover all of phase space parton showers implement strong ordering as $Q_{\text{emit}}^2 > Q_{\text{split}}^2$ and recoil effects may appear, especially when the involved particles are as heavy as the electroweak gauge bosons. The $2 \rightarrow 3$ kinematic map used by the antenna shower conserves the invariant mass of the original two-particle system, so by using the probability in eq. (5.9) the invariant mass of the system of emitter + vector boson that was most important in the emission process is most often conserved. In [29] this effect is called ‘kinematic back-reactions’ and it is accounted for as a multiplicative factor of the branching kernels. We instead choose to implement it as a spectator selection probability.

5.3 Bosonic Interference

A unique type of interference effect appears in the electroweak shower, namely the overlap between photons and transversely polarized Z -bosons or Higgs bosons and longitudinally polarized Z -bosons [64]. In [29], a procedure involving mixed branching kernels and evolution of a density matrix is described. While this procedure is physically accurate, it is not straightforward to combine with the definite intermediate states that appear as part of the shower evolution and may lead to a computationally expensive algorithm. In this work, we instead opt for a simple approach that attempts to incorporate the most important physical effect at little computational cost.

We consider the electroweak shower evolving an f final state and ending up with an $f f' \bar{f}'$ configuration. Using the treatment of spins described in the previous paragraph, the two shower histories $f \rightarrow f \gamma \rightarrow f f' \bar{f}'$ and $f \rightarrow f Z_T \rightarrow f f' \bar{f}'$ contribute to this final state separately for some particular spin configuration. For different helicities, the intermediate particles may instead be h and Z_L . In a shower with full spin-interference effects all of these shower histories would contribute.

Without any treatment of bosonic interferences, the shower approximation to such a $1 \rightarrow 3$ branching process can be described diagrammatically as

$$\begin{aligned}
 & \left| \begin{array}{c} \text{Feynman diagram: } f \rightarrow f \gamma \rightarrow f f' \bar{f}' \\ \text{Feynman diagram: } f \rightarrow f Z_T \rightarrow f f' \bar{f}' \end{array} \right|^2 = \left| \begin{array}{c} \text{Feynman diagram: } f \rightarrow f \gamma \rightarrow f f' \bar{f}' \\ \text{Feynman diagram: } f \rightarrow f Z_T \rightarrow f f' \bar{f}' \end{array} \right|^2 \\
 & + \left| \begin{array}{c} \text{Feynman diagram: } f \rightarrow f \gamma \rightarrow f f' \bar{f}' \\ \text{Feynman diagram: } f \rightarrow f Z_T \rightarrow f f' \bar{f}' \end{array} \right|^2
 \end{aligned} \tag{5.11}$$

where the two separate contributions correspond to the probabilities for the shower to emit either a photon or a Z -boson, and its subsequent splitting. To adjust for the interference contributions, we add an event weight when a neutral vector boson splitting occurs. This event weight may be expressed diagrammatically as

$$w_{\text{BI}} = \sum_i \frac{\left| \begin{array}{c} \text{Feynman diagram: } f \rightarrow f \gamma \rightarrow f f' \bar{f}' \\ \text{Feynman diagram: } f \rightarrow f Z_T \rightarrow f f' \bar{f}' \end{array} \right|^2}{\left| \begin{array}{c} \text{Feynman diagram: } f \rightarrow f \gamma \rightarrow f f' \bar{f}' \\ \text{Feynman diagram: } f \rightarrow f Z_T \rightarrow f f' \bar{f}' \end{array} \right|^2 + \left| \begin{array}{c} \text{Feynman diagram: } f \rightarrow f \gamma \rightarrow f f' \bar{f}' \\ \text{Feynman diagram: } f \rightarrow f Z_T \rightarrow f f' \bar{f}' \end{array} \right|^2}, \tag{5.12}$$

and similar for h/Z_L interference. The index i runs over all electroweak charges that could have emitted the neutral boson. Note that if the initial fermion is massive, multiple fermionic spin states can contribute to the photon and Z emission diagrams. For example, the fermion may start out with a positive helicity and emit a neutral vector boson without flipping its spin, or it may start out with negative helicity and emit a vector boson while flipping to positive helicity. This type of interference between spin states is not included elsewhere in the shower, and as such the contributions are summed over incoherently in eq. (5.12). For similar reasons, interference between transverse and longitudinal intermediate vector bosons is not accounted for.

The weight of eq. (5.12) corrects the branching kernels of the shower, but not the higher-order corrections included in the Sudakov factor. In that sense, this reweighting procedure is not as accurate as a treatment that involves evolution of density matrices, but it is computationally much simpler and does not lead to the presence of mixed states in the event record. An inclusion of a correction factor like eq. (5.12) during the shower evolution is not straightforward because the neutral boson emission rates have to be modified prior

to the splitting taking place. We also point out that eq. (5.12) has an upper bound of 2, and as such there is little danger of wildly fluctuating weights leading to inefficiencies.

5.4 Overestimate Determination

One technical problem with the implementation of the parton shower is related to finding suitable overestimates, which are required for the Sudakov veto algorithm [65–67] commonly used to generate the shower evolution. The electroweak branching kernels are defined in terms of spinor products, while the antenna phase space is given in terms of inner products of the post-branching momenta. The task of determining overestimates for the branching kernels is consequently not straightforward. Furthermore, due to the sheer volume of available electroweak branchings, it is desirable to automate this procedure.

Final-state branchings are only allowed to recoil against other final-state particles, which are selected probabilistically as described in the previous section. The antenna phase space is given by

$$d\Phi_{\text{ant}}^{\text{FF}} = \frac{1}{16\pi^2} m_{IK}^2 \lambda^{-\frac{1}{2}}(m_{IK}^2, m_I^2, m_K^2) ds_{ij} ds_{jk} \frac{d\varphi}{2\pi}, \quad (5.13)$$

where I is the brancher and K is the spectator. All final-state electroweak branching kernels are overestimated by a parameterized function

$$\begin{aligned} \mathcal{O}^{\text{FF}} &= c_1^{\text{FF}} \frac{1}{|Q^2|} + c_2^{\text{FF}} \frac{1}{|Q^2|} \frac{E_{IK}(E_{IK} + |\vec{p}_{IK}|)}{s_{ij} + s_{ik} + m_i^2} \\ &+ c_3^{\text{FF}} \frac{1}{|Q^2|} \frac{E_{IK}(E_{IK} + |\vec{p}_{IK}|)}{s_{ij} + s_{jk} + m_j^2} + c_4^{\text{FF}} \frac{m_I^2}{(Q^2)^2}. \end{aligned} \quad (5.14)$$

In terms of the antenna phase space variables, the ordering scale is

$$|Q^2| = |s_{ij} + m_i^2 + m_j^2 - m_I^2|. \quad (5.15)$$

The term multiplying c_1^{FF} reflects the general $1/|Q^2|$ behaviour of the collinear limits of many branching kernels. The second and third terms also incorporate the soft behaviour mostly associated with vector boson emission. In the center-of-mass frame of the pair I and K , the energies of the post-branching momenta are given by

$$E_i^{\text{CM}} = \frac{s_{ij} + s_{ik} + m_i^2}{2m_{IK}} \quad \text{and} \quad E_j^{\text{CM}} = \frac{s_{ij} + s_{jk} + m_j^2}{2m_{IK}}, \quad (5.16)$$

where $m_{IK}^2 = (p_I + p_K)^2$. By Lorentz boosting, an underestimate for these energies in the lab frame can be found. They are

$$E^{\text{Lab}} = \frac{E^{\text{CM}} E_{IK}^{\text{Lab}} + \vec{p}^{\text{CM}} \cdot \vec{p}_{IK}^{\text{Lab}}}{m_{IK}} \geq E^{\text{CM}} \frac{E_{IK}^{\text{Lab}} - |\vec{p}_{IK}^{\text{Lab}}|}{m_{IK}} = E^{\text{CM}} \frac{m_{IK}}{E_{IK}^{\text{Lab}} + |\vec{p}_{IK}^{\text{Lab}}|}. \quad (5.17)$$

The second and third term of eq. (5.14) thus contain the ratios $E_{IK}/E_i \sim 1/z$ and $E_{IK}/E_j \sim 1/(1-z)$ expressed in the invariants that appear in the phase space using the above underestimate. In practice, these terms can lead to problematic behaviour when

$E_{IK}/m_{IK} \gg 1$, corresponding to a strongly boosted brancher-recoiler pair. We therefore restrict the spectator selection to never select pairs that have a very large boost. The term multiplying c_4^{FF} represents the mass corrections that may be present for massive branchers. The contribution of post-branching masses are typically negative, and therefore do not improve the overestimate much.

Initial-state branchings are only allowed to recoil against other initial states. In this case, the antenna phase space is

$$d\Phi_{\text{ant}}^{\text{II}} = \frac{1}{16\pi^2} \frac{x_A^2 x_B^2}{x_a^2 x_b^2} \frac{1}{s_{AB}} ds_{aj} ds_{bj} \frac{d\varphi}{2\pi}, \quad (5.18)$$

where A branches to a and j , and B is the recoiler. The electroweak shower currently only implements vector boson emission from fermions in the initial state, which are treated as massless by Vincia. The ordering variable is crossed into the initial state to give

$$Q^2 = s_{aj} - m_j^2. \quad (5.19)$$

An absolute value qualification is not required here since resonance type branchings do not occur in the initial state. A sufficient overestimate is

$$\mathcal{O}^{\text{II}} = c_1^{\text{II}} \frac{1}{Q^2} \frac{s_{ab}}{s_{AB}} + c_2^{\text{II}} \frac{1}{Q^2} \frac{x_A^2 s_{ab}^2}{x_A s_{bj} (s_{ab} - s_{bj}) + x_B s_{aj} (s_{ab} - s_{aj})}. \quad (5.20)$$

The factor s_{ab}/s_{AB} accounts for the additional factor of $1/z$ that shows up in the Altarelli-Parisi splitting kernels when crossed to the initial state. The second term represents the $1/(1-z)$ contribution that may appear for vector boson emissions. It is constructed by making use of the fact that the vector $E_a p_b + E_b p_a$ is at rest in the lab frame, and thus

$$(p_a^0 p_b + p_b^0 p_a) \cdot p_j \propto E_j. \quad (5.21)$$

The parameters c_1^{FF} through c_4^{FF} , c_1^{II} and c_2^{II} are automatically determined for all possible branchings in the electroweak shower. To do that, brancher-recoiler pairs are generated from antennae with randomly chosen invariant masses. Branchings are then generated with a distribution $1/|Q^2|$ for the final state or $s_{ab}/s_{AB} 1/Q^2$ for the initial state to roughly model the branching kernel behaviour. For every event i , the value of the branching kernel B_i as well as the terms A_{ij} multiplying the parameters c_j are stored. The problem of finding suitable values for the overestimate parameters can then be formulated as

$$\begin{aligned} & \text{Minimize } \sum_{i=1}^n (\mathbf{A}\mathbf{c})_i - B_i \\ & \text{subject to } (\mathbf{A}\mathbf{c})_i \geq B_i \text{ and } \mathbf{c} \geq 0. \end{aligned} \quad (5.22)$$

The minimization condition minimizes the average difference between the branching kernel and its overestimate. The constraints ensure the overestimate is larger than the branching kernel for all samples and the parameters are positive definite. The above problem is an instance of a mathematical optimization problem known as *linear programming*, for which many libraries are available. We make use of the Python [68] package PuLP [69].

5.5 Overview of the Shower Algorithm

We conclude this section with a short description of the complete shower algorithm. Branching kernels are constructed using the formalism described in section 3 for all possible electroweak branchings and all helicity configurations. Overestimates are found using the optimization algorithm of subsection 5.4, where the post-branching helicities are summed over. This leaves a total of 277 types of final-state branchings, of which 74 are resonance decays, and 90 types of initial-state branchings.

As the shower initializes, a recoiler is selected for all final-state particles that have $SU(2)$ or $U(1)$ charges making use of the selection probability described in subsection 5.2. Initial-state branchers are always paired with the other initial-state particle, recoiling against the entire event.

While the shower runs, electroweak branchings compete against the QCD branchings generated by Vincia. The overestimates are used to generate trial branchings which are accepted or rejected through the usual Sudakov veto algorithm. For resonance decay branchings, the procedure outlined in subsection 5.1 is used to match the shower to a Breit-Wigner distribution. We make use of the same kinematic maps as Vincia, and first-order running of the electroweak coupling constant is incorporated as part of the veto procedure. A difference between the electroweak shower and the QCD shower, and a definite downside of the spinor-helicity formalism is that the electroweak branching kernels are not functions of the variables that appear in the antenna phase space factorizations eq. (5.13) and eq. (5.18). This means that the kinematic mapping always has to be performed before the veto probability can be computed. Wherever applicable, the bosonic interference weight eq. (5.12) is included. After accepting a branching, a helicity state is selected with probability

$$\mathcal{P}_{\lambda_I, \lambda_i, \lambda_j} = \frac{B_{\lambda_I, \lambda_i, \lambda_j}(p_I, p_i, p_j)}{\sum_{\lambda_i, \lambda_j} B_{\lambda_I, \lambda_i, \lambda_j}(p_I, p_i, p_j)}. \quad (5.23)$$

The QCD shower and the electroweak shower run interleaved until the QCD cutoff scale is reached, after which only QED radiation is simulated.

6 Results

6.1 Branching Spectra

To get a general sense for the branching rates predicted by the electroweak shower, we consider emission spectra for several highly energetic particles that have an electroweak charge. Figures 2, 3, 4 and 5 show the invariant mass distribution for the first branching of a left-handed τ and top, a transverse W^+ boson and a Higgs. All particles are produced at an energy of 1 TeV together with a recoiler that is uncharged under electroweak interactions. For photon emissions, a cutoff around Λ_{QCD} is imposed. All other branchings are automatically regulated by the particle masses. For all resonance decay branchings, the sampled matching procedure outlined in section 5.1 is used.

Figure 2 shows the branching spectrum of a negative-helicity τ . The two dominant photon production channels are those where the τ helicity is conserved. The mass-suppressed

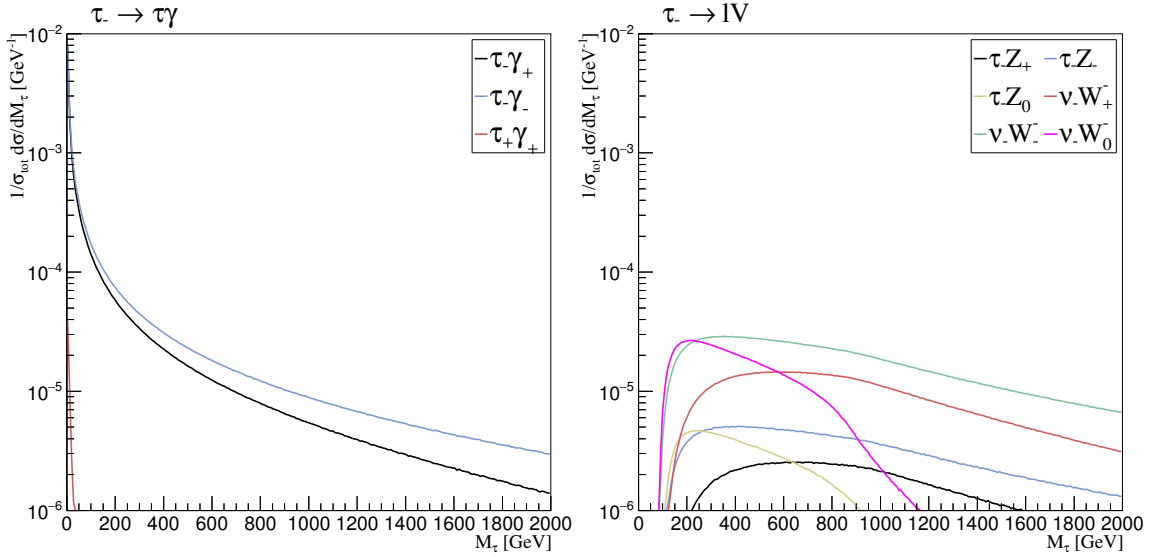


Figure 2. Branching spectra of a 1 TeV τ_- to $\tau\gamma$ (left) and τZ and $\nu_\tau W^-$ (right).

spin-flip mode only contributes at very small invariant masses, as is to be expected from the branching kernel behaviour of $m_\tau^2/(Q^2)^2$. The other spin-flip mode is highly suppressed in the collinear limit as is indicated in Table 1. For the emission of other vector bosons, the spin-flip contributions do not become sufficiently enhanced to show up before the kinematic limit is reached. The longitudinal vector boson emission channels have a characteristic form which looks very similar for the W_0^- and the Z_0 channels, and which becomes comparable to the transverse channels at scales close to the kinematic limit.

Figure 3 shows the branching spectrum of a negative-helicity top. The left graph displays the resonance branchings as generated by the sampled matching procedure outlined in subsection 5.1. The right and bottom graphs show all other branchings that are not of the resonance decay type. Spin-flip modes now show up for $t \rightarrow bW^+$, $t \rightarrow tZ$ and $t \rightarrow t\gamma$ due to the large top mass, and they show the expected $m_t^2/(Q^2)^2$ scaling with the emission scale. The ‘natural’ mode of spin-flip Higgs emission is relatively flat compared with the fermion mass scaling mode of Higgs emission without spin flip.

Figure 4 shows the branching spectrum of a transverse W^+ . Resonance peaks only appear for decays to negative-helicity states due to their small masses. The branchings $W_+^+ \rightarrow t\bar{b}$ with a spin-flipped top do occur on the other hand. The $W_+^+ \rightarrow W^+Z$ and $W_-^+ \rightarrow W^+\gamma$ channels are dominated by the all-positive helicity configuration because of its $1/z(1-z)$ scaling in the collinear limit as can be seen in Table 3. The modes to opposite transverse helicities are almost identical for the W^+Z channels due to symmetry in the collinear limit and almost identical mass, but they are widely different for low scales in the $W^+\gamma$ channels. This is caused by the $z^3/(1-z)$ and $(1-z)^3/z$ scaling of the collinear limits, where the photon can attain a very small collinear momentum fraction while that of the W^+ is constrained by its mass. The single-longitudinal channels in W^+Z are also almost identical for very similar reasons. The $W_0^+Z_0$ is a mode that is related to the Goldstone

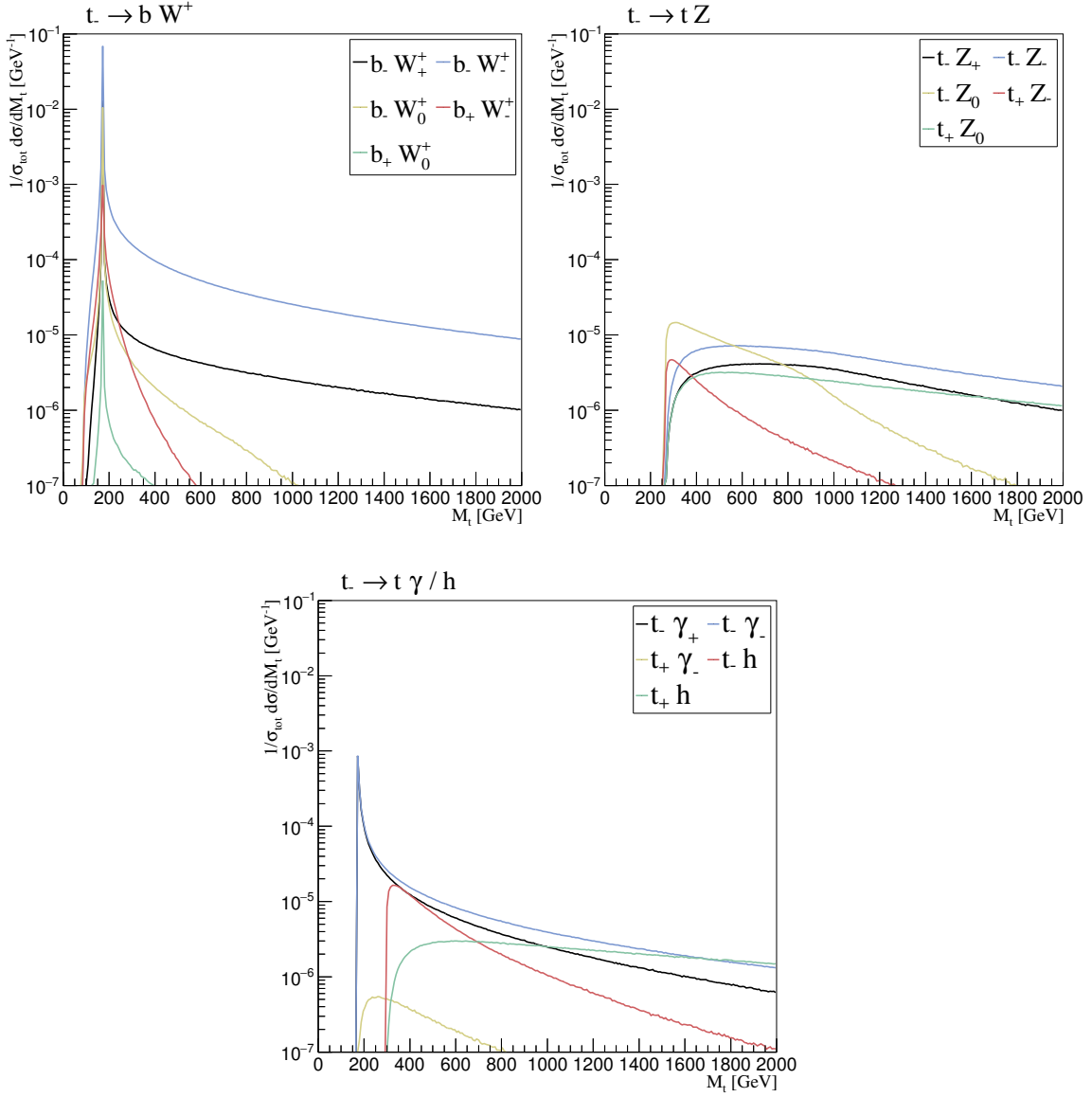


Figure 3. Branching spectra of a 1 TeV top quark to bW^+ (left), tZ (right) and $t\gamma/h$ (bottom).

bosonic part of the W^+ and Z , and it can be seen to be very similar to the W_0^+h channel. On the other hand, the W_+^+h mode differs significantly from the $W_+^+Z_0$ channel because it is dominated by the vectorial part of the longitudinal polarization.

Figure 5 shows the branching spectrum of a Higgs. The only significant resonance decay channels are $b_\pm\bar{b}_\pm$ and $\tau_\pm\bar{\tau}_\pm$ as may be expected due to the coupling to the fermion mass and the Higgs spin zero nature. On the other hand, the mass-suppressed $t_\pm\bar{t}_\pm$ channel is comparable with the natural $t_\pm\bar{t}_\pm$ channel. All channels to W^+W^- and ZZ are almost identical since their branching kernels only differ in the gauge boson mass and a factor of $1/c_w$ in the coupling. Also included is the $h \rightarrow hh$ cubic Higgs coupling which is proportional

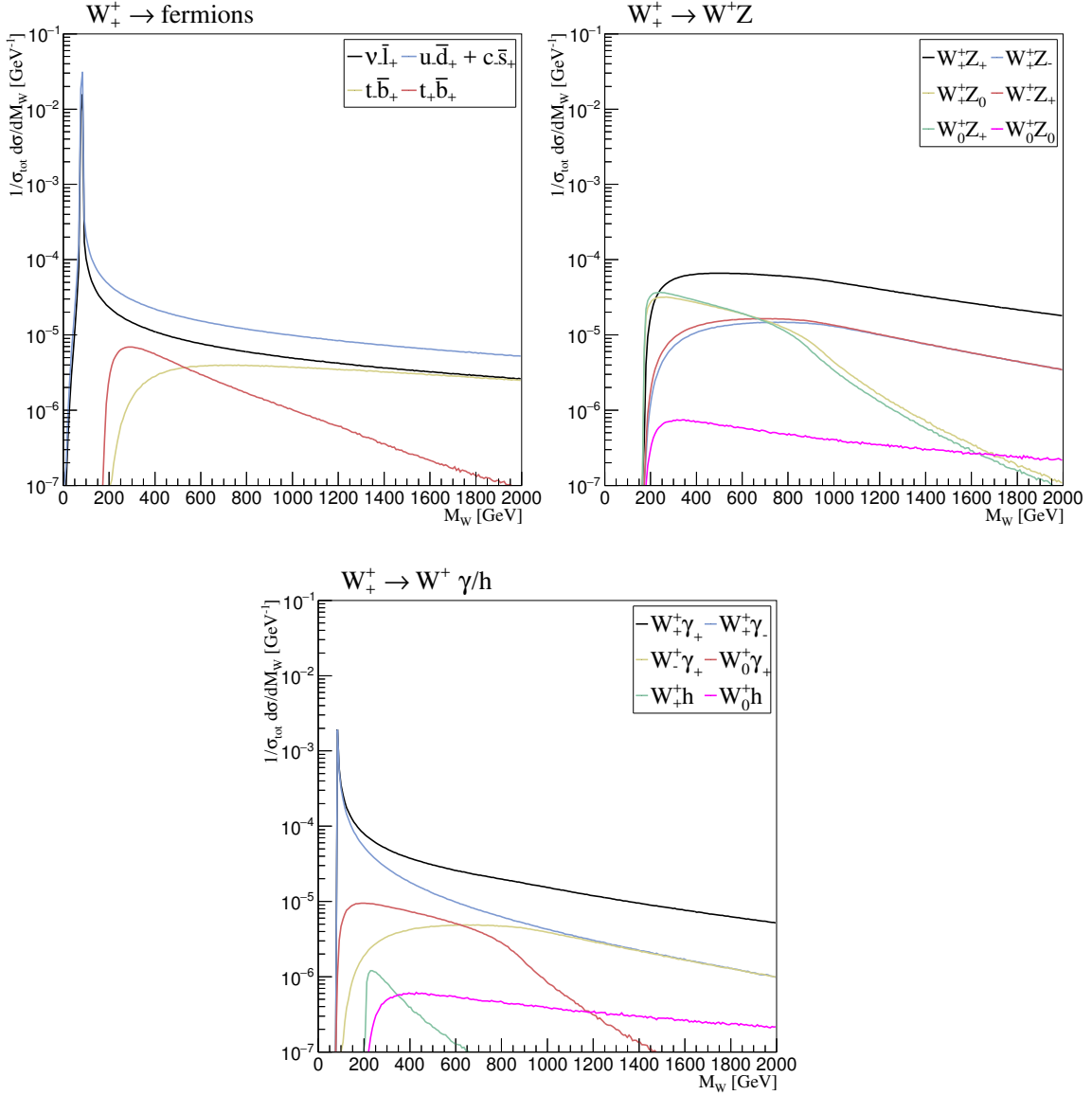


Figure 4. Branching spectra of a 1 TeV W^+ to fermions (left), W^+Z (right) and $W^+\gamma/h$ (bottom).

to the Higgs mass m_h , or equivalently the Higgs self-coupling λ . This is the only branching where it makes an appearance, and it can be seen to provide a significant contribution to the total branching rate.

6.2 Bosonic Interference

We now consider the effect of the application of the bosonic interference factor described in section 5.3. Figure 6 shows rates for the shower histories $e_- \rightarrow e_- \gamma/Z_T \rightarrow e_- X$ and $e_+ \rightarrow e_+ \gamma/Z_T \rightarrow e_+ X$ using a similar setup as in the previous subsection, but starting from a 10 TeV source electron. Multiple interesting features appear when the bosonic interference weight eq. (5.12) is included. The most striking difference occurs for the W^+W^- channel,

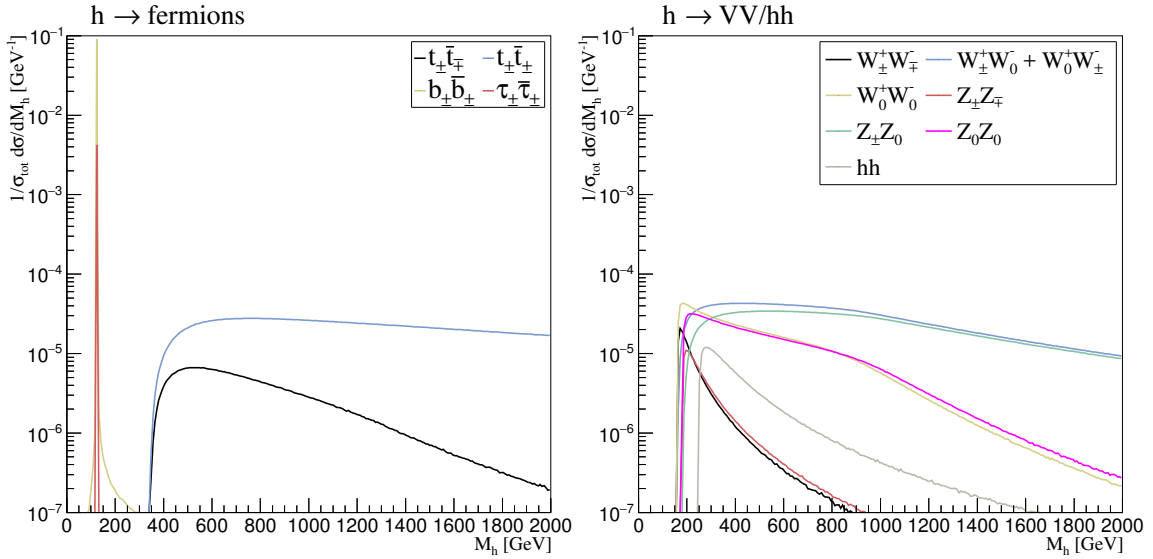


Figure 5. Branching spectra of a 1 TeV Higgs boson to fermions (left) and VV/hh (right).

where the bosonic interference causes an increase in case of the e_- , but a major decrease in case of the e_+ . This may be understood by considering the structure of the interfering branching amplitudes. Factoring out coupling constants and other kinematic components, the interference is proportional to

$$\frac{1}{M_{WW}^2} + \frac{c_w}{s_w} \frac{1}{4s_w c_w} (1 - 4s_w^2 - \lambda_e) \frac{1}{M_{WW}^2 - m_z^2 + im_z \Gamma_z}, \quad (6.1)$$

where the factor c_w/s_w comes from the ZWW -coupling and λ_e is the electron helicity. The second term in brackets interferes destructively with the photon contribution for sufficiently large values of M_{WW} , and the remaining terms in the Z contribution cancel for $\lambda = 1$.

The effects of the bosonic interference factor on charged fermion rates close to the Z peak may be understood through a similar argument. The rates close to the Z peak are significantly affected by the simplified and preliminary method of matching to resonance decays as described in section 5.1, and will be improved upon in [63]

6.3 Electroweak Corrections to Proton Collision Processes

We finally consider the parton shower predictions of electroweak corrections to some common proton collision processes at LHC energies. Since the weak vector bosons produced by the electroweak shower at high energies are massive and thus observable, they may provide a rich environment for phenomenological studies including kinematic effects on the hard scattering, jet substructure due to vector boson decay inside jet cones and external high-energy jet and lepton production.

With the goal of examining the general size of the effects of the electroweak shower in common LHC processes, we generate dijet and W^+ plus jet events at $\sqrt{s} = 14$ TeV using the default tune of Pythia 8.2 [24] and the NNPDF2.3 sets [70]. Figure 7 shows the

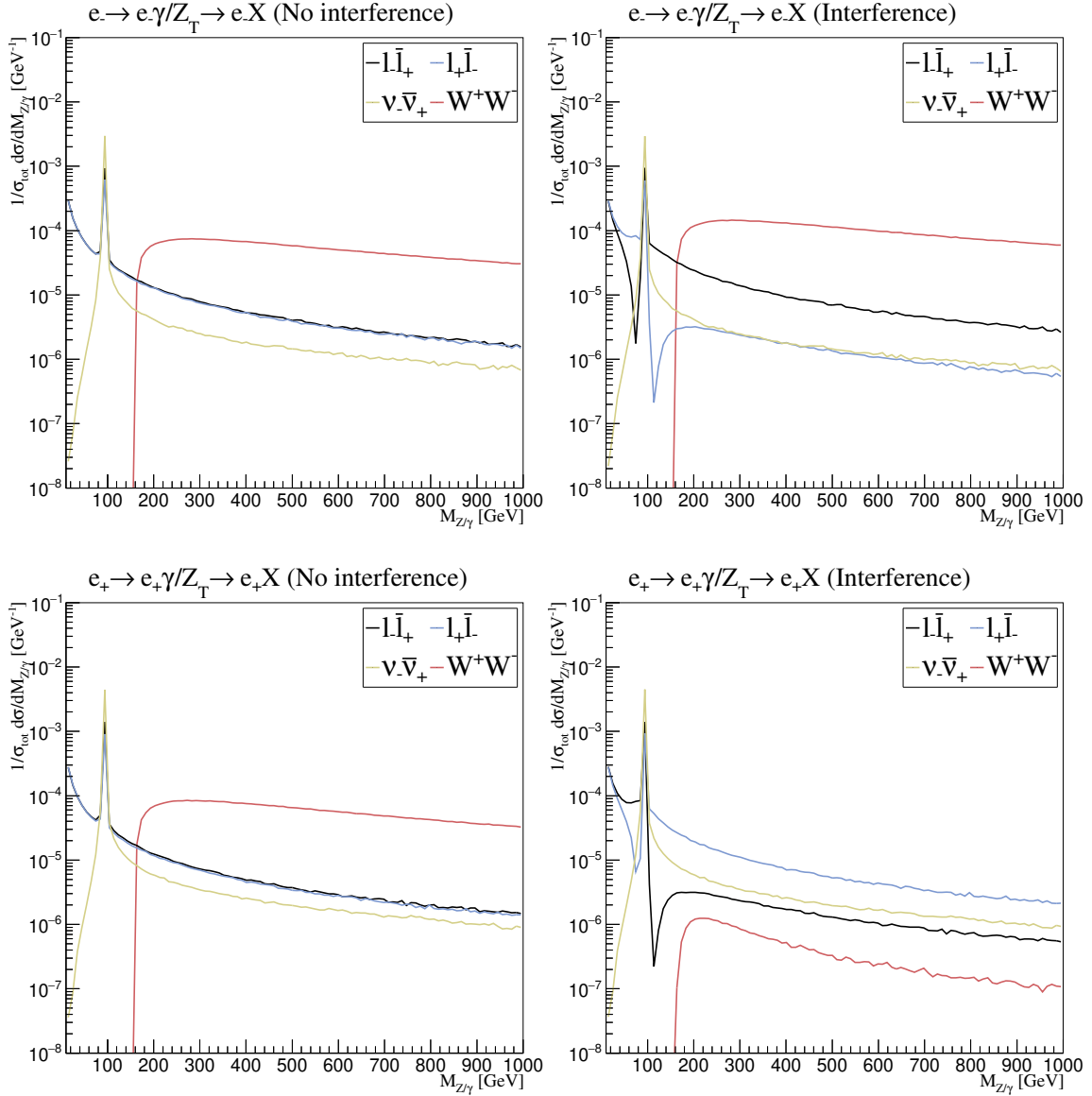


Figure 6. Differential rates of the shower histories $e_- \rightarrow e_- \gamma / Z_T \rightarrow e_- X$ (top) and $e_+ \rightarrow e_+ \gamma / Z_T \rightarrow e_+ X$ (bottom) without (left) and with (right) the bosonic interference correction. The showers are initiated from a 10 TeV electron with a neutral recoiler.

approximate electroweak virtual corrections as predicted by the Pythia electroweak shower, which only incorporates vector boson emission from fermions, and the Vincia electroweak shower. The virtual corrections may be estimated by counting the events that contain at least one weak vector boson emission. The probability for the shower to produce no additional weak bosons is given by the Sudakov factor

$$\Delta_{\text{EW}} = 1 - \mathcal{O}(\alpha), \quad (6.2)$$

and thus the $\mathcal{O}(\alpha)$ corrections are given by the probability for at least one weak boson

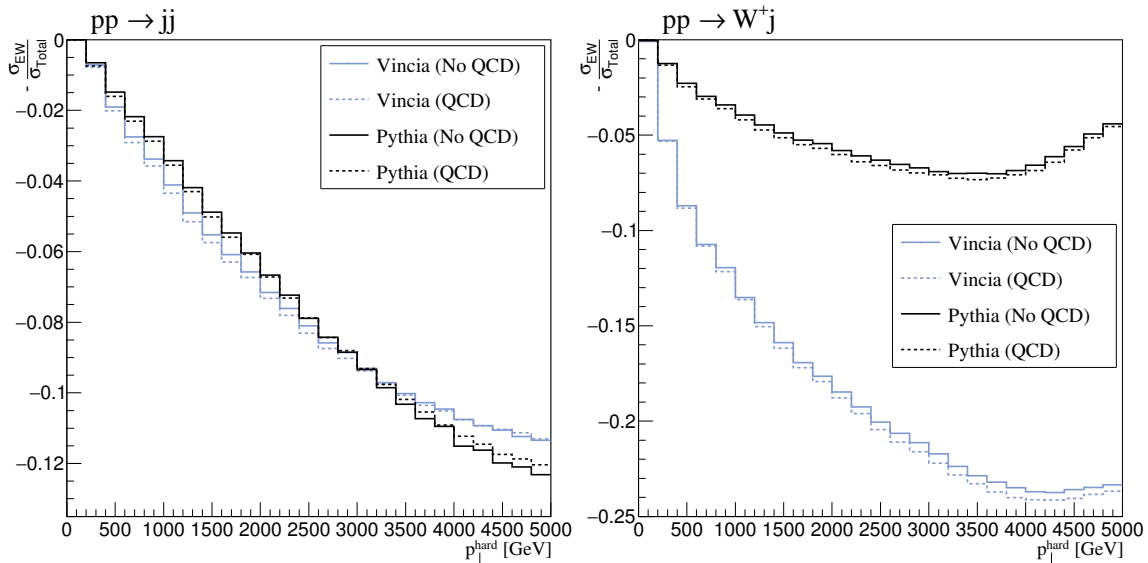


Figure 7. Electroweak shower approximation of electroweak virtual corrections to exclusive dijet production and exclusive W^+ + jet production at center-of-mass energy $\sqrt{s} = 14$ TeV as a function of the transverse momentum of the hard scattering process p_{\perp}^{Hard} . The solid line corresponds to the parton shower prediction without the QCD shower, while the dashed line shows the effect of interleaving with QCD radiation.

emission. Virtual corrections to these processes were calculated in for example [14, 15] for exclusive dijet production and in [17, 18] for vector boson production. For dijet production, the results of the showers are similar and are comparable in size to analytic results found in [14, 15]. In the case of W^+ plus jet production the substantial difference between the showers is caused by the absence of the Yang-Mills vector boson coupling in the Pythia shower. However, the Vincia shower still underestimates the analytical results significantly. In [29] a similar calculation was performed using a purely final-state electroweak shower. The effects of initial-state radiation were approximated by generating $pp \rightarrow W^+q$ and squaring the Sudakov factor associated with the quark. We however find that the contribution to the weak boson emission rates of the initial-state quarks is much smaller than that of the final state. At large x and high scales the PDFs are predominantly quark-like and the hard scattering is dominated by $q\bar{q}' \rightarrow W^+g$. Furthermore, the initial-state phase space at large x is small. These effects lead to the decrease in the estimated virtual correction at large p_{\perp}^{Hard} .

Also shown in Figure 7 are the results of interleaving the electroweak shower with the QCD showers of Pythia and Vincia. In the strongly ordered limit shower branchings are unaffected by subsequent branchings, but subleading effects due to the kinematics and the creation of weakly charged quarks still lead to minor differences.

Figure 8 shows the average number of weak boson emissions of the showers. In W^+ plus jet production the first purely vector boson branching is always $W^+ \rightarrow W^+Z$ explaining the large increase in the Z boson emission rates. Similarly, Pythia's W^+ rate is small since

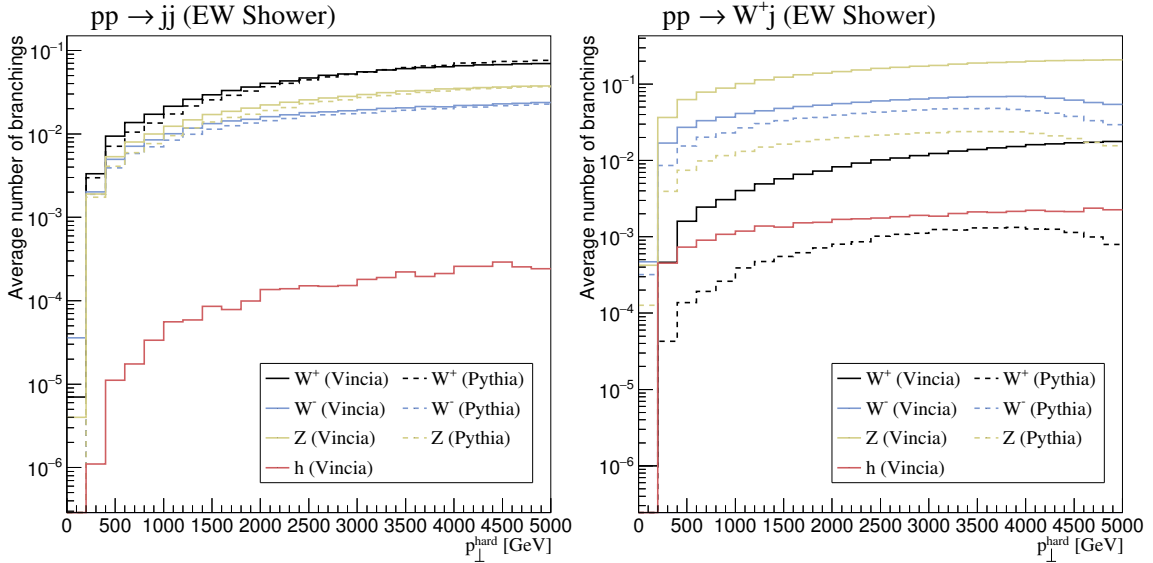


Figure 8. Average number of weak boson emissions in exclusive dijet production and exclusive W^+ + jet production at center-of-mass energy $\sqrt{s} = 14$ TeV as a function of the transverse momentum of the hard scattering process p_{\perp}^{Hard} .

the final-state quark is always down-type. The increase in the Vincia shower is thus caused entirely by secondary emissions from prior weak vector boson emissions.

7 Conclusion and Discussion

The effects of weak boson radiation are known to become significant already at LHC energies, in particular with the upcoming luminosity upgrade, and will be even more relevant at future colliders. One of the major challenges of the construction of such a shower is the calculation of the relevant branching kernels, which in this paper was done using the spinor-helicity formalism. Compared with QCD, the electroweak theory involves many theoretical subtleties that have to be handled carefully. One major issue is the chiral nature of the electroweak theory, which forces the shower to be helicity-dependent and leads to a large number of possible types of branchings. Longitudinal polarizations appear for the massive weak gauge bosons, which lead to gauge-dependent unitarity violating terms in the calculation of branching kernels that have to be removed manually. The collinear limits of the computed branching kernels are found to be in agreement with the results of [29]. The electroweak shower also includes many branchings that would usually be considered to be decays of resonances, in which case the distribution follows a Breit-Wigner peak. A strategy to match the parton shower to a resonance decay was proposed, but this may likely be improved upon by a better understanding of the interplay between the virtual corrections contained in the Sudakov factor and the decay width. A more sophisticated treatment of this matching is beyond the scope of this paper, and will be the topic of future study [63]. Further electroweak effects added to the shower include a recoiler selection

procedure that compensated for recoil effects of previous branchings and treatment of bosonic interference effects.

In the text, several features that are currently lacking from the electroweak shower were already pointed out. They include topics such as soft interference, spin interference and the option to select an ordering scale that is more closely aligned with the transverse momentum ordering used by the QCD part of the Vincia shower. The branching kernels defined directly in terms of spinor products come with several advantages, such as the ability to incorporate the bosonic interference weight eq. (5.12) and the recoil selection procedure of section 5.2. However, generating branchings in the electroweak shower with these kernels suffers from numerical issues associated with the mismatch with the phase space factorization, as was pointed out in section 5.4. To bring the electroweak shower in line with the rest of the Vincia QCD evolution in the future, we intend to sample branchings using antenna that capture the collinear limits as defined in section 4, while maintaining the spinor-helicity kernels for the applications mentioned above.

We finally point out some further possible improvements that are closely related to further details of the electroweak sector. One is the inclusion of the CKM quark-mixing matrix [71, 72]. In the context of the shower, it would contribute by allowing branchings like $d \rightarrow cW^-$ or $t \rightarrow sW^+$. Because of the weak universality condition

$$\sum_i |V_{ik}|^2 = \sum_k |V_{ik}|^2 = 1 \quad (7.1)$$

the squared matrix elements $|V_{ik}|^2$ can be interpreted as probabilities multiplying the W -emission branching kernels. The impact of the CKM matrix is not expected to be large since the off-diagonal terms of the third-generation row and column are close to zero. The other off-diagonal terms are not as small, but they mix quarks that are treated as massless in Vincia anyway.

One other peculiar property of the electroweak theory is the appearance of Bloch-Nordsieck violation [10, 73]. The parton shower formalism is fundamentally based on the principle of unitarity and the cancellation of infrared divergences between real and virtual corrections. Since the electroweak vector bosons are massive, divergences associated with their emission are mass-regulated. The flavour-changing nature of W -boson emission from the initial state spoils the exact cancellation of the infrared divergences and some mass-regulated logarithms may be left-over. This phenomenon is called Bloch-Nordsieck violation, and it was already pointed out in the electroweak shower implementation in Pythia in [22].

There is no straightforward method to incorporate these violations in the shower formalism, since they explicitly break unitarity. However, Bloch-Nordsieck violations are not particularly significant at the LHC [10, 15]. They only appear for W -radiation from the initial state, and only when both initial-state particles are quarks with the correct $SU(2)$ charge to emit a W boson.

Finally, hard processes initiated by vector bosons have been considered for a long time [74, 75]. PDF sets with QED corrections have been available for some time [76–78], and recent progress was made towards PDFs with complete electroweak corrections [79–81]. The

current shower implementation only allows for the emission of vector bosons from the initial state. The calculation of the other required initial-state branching kernels is in principle as straightforward as the calculation of those available already, but an implementation in the Pythia framework is likely not simple.

Acknowledgments

We are grateful to Helen Brooks and Peter Skands for many useful discussions and help with the implementation in the Vincia parton shower. R. V. acknowledges support by the Foundation for Fundamental Research of Matter (FOM) via program 156 'Higgs as Probe and Portal' and by the Science and Technology Facilities Council (STFC) via grant award ST/P000274/1.

A Relevant Feynman Rules of the Electroweak Theory

This appendix lists the Feynman rules of the electroweak theory that are relevant for the calculation of branching amplitudes. We elect to make use of a practical notation for the electroweak Feynman rules. It makes for simpler results, but some of the underlying group structure is obfuscated. We work in the unitary gauge, which has propagators

$$\begin{aligned}
 \text{---}\xrightarrow{p}\text{---} &= i \frac{\not{p} + m}{p^2 - m^2 + im\Gamma} \\
 \text{~~~~~} &= i \frac{-g^{\mu\nu} + \frac{p^\mu p^\nu}{m^2}}{p^2 - m^2 + im\Gamma} \\
 \text{-----} &= i \frac{1}{p^2 - m^2 + im\Gamma}.
 \end{aligned} \tag{A.1}$$

	v			a			g_V
	γ	W	Z	γ	W	Z	
d	$-\frac{1}{3}e$	$\frac{-e}{\sqrt{8s_w}}$	$\frac{-e}{4s_w c_w} \left(1 - \frac{4}{3}s_w^2\right)$	0	$\frac{-e}{\sqrt{8s_w}}$	$\frac{-e}{4s_w c_w}$	$-e$
u	$\frac{2}{3}e$	$\frac{-e}{\sqrt{8s_w}}$	$\frac{e}{4s_w c_w} \left(1 - \frac{8}{3}s_w^2\right)$	0	$\frac{-e}{\sqrt{8s_w}}$	$\frac{e}{4s_w c_w}$	$-e\frac{c_w}{s_w}$
e	$-e$	$\frac{-e}{\sqrt{8s_w}}$	$\frac{-e}{4s_w c_w} \left(1 - 4s_w^2\right)$	0	$\frac{-e}{\sqrt{8s_w}}$	$\frac{-e}{4s_w c_w}$	gh
ν	0	$\frac{-e}{\sqrt{8s_w}}$	$\frac{e}{4s_w c_w}$	0	$\frac{-e}{\sqrt{8s_w}}$	$\frac{e}{4s_w c_w}$	$-e\frac{m_W}{s_w}$

Table 5. Values of the coupling constants

The vertex interactions are

$$\begin{aligned}
& \begin{array}{c} \text{---} V \\ | \\ \text{---} f \quad \text{---} f' \end{array} = i(v + a\gamma^5)\gamma^\mu & \begin{array}{c} | h \\ | \\ \text{---} f \quad \text{---} f \end{array} = i\frac{e}{2s_w}\frac{m_f}{m_W} \\
& \begin{array}{c} \text{---} V_1 \\ | \\ \text{---} h \quad \text{---} V_2 \end{array} = ig_h g^{\mu\nu} & \begin{array}{c} | h \\ | \\ \text{---} h \quad \text{---} h \end{array} = -i\frac{3}{2}\frac{m_h^2}{m_w s_w} \\
& \begin{array}{c} \text{---} V_1 \\ | \\ p_1^\mu \text{---} \\ | \\ p_3^\alpha \text{---} V_3 \quad p_2^\nu \text{---} V_2 \end{array} = ig_V Y(p_1, \mu, p_2, \nu, p_3, \alpha) \tag{A.2}
\end{aligned}$$

where

$$Y(p_1, \mu, p_2, \nu, p_3, \alpha) = (p_1 - p_2)^\alpha g^{\mu\nu} + (p_2 - p_3)^\mu g^{\nu\alpha} + (p_3 - p_1)^\nu g^{\mu\alpha} \tag{A.3}$$

is the Yang-Mills vertex. As usual, the weak mixing angle is defined as

$$c_w \equiv \cos \theta_w = \frac{m_W}{m_Z} \quad s_w \equiv \sin \theta_w. \tag{A.4}$$

The coupling constants are defined in Table 5.

B Branching amplitudes

All branching amplitudes are multiplied by a propagator factor

$$\frac{1}{Q^2}. \tag{B.1}$$

where

$$Q^2 = \begin{cases} 2p_i \cdot p_j + m_i^2 + m_j^2 - m_I^2 & \text{(Final State)} \\ 2p_a \cdot p_j - m_j^2 & \text{(Initial State)}. \end{cases} \quad (\text{B.2})$$

B.1 Vector Boson Emission

We define the prefactors

$$\begin{aligned} A_{\perp}^{\text{emit}} &= \frac{1}{2\sqrt{2}} \frac{\lambda}{\sqrt{p_i \cdot k_i} \sqrt{p_{ij} \cdot k_{ij}} p_j \cdot k_j} \\ A_L^{\text{emit}} &= \frac{1}{2} \frac{1}{m_j} \frac{1}{\sqrt{p_i \cdot k_i} \sqrt{p_{ij} \cdot k_{ij}}}. \end{aligned} \quad (\text{B.3})$$

B.1.1 Vector Boson Emission from Fermion

$$\begin{aligned} M^{f \rightarrow f'V}(\lambda, \lambda, \lambda) &= A_{\perp}^{\text{emit}} \left[(v - \lambda a) S_{-\lambda}(k_i, p_i, p_j, k_j) S_{-\lambda}(k_j, p_{ij}, k_{ij}) \right. \\ &\quad \left. + (v + \lambda a) m_i m_I S_{-\lambda}(k_i, k_j) S_{-\lambda}(k_j, p_j, k_{ij}) \right] \\ M^{f \rightarrow f'V}(\lambda, \lambda, -\lambda) &= A_{\perp}^{\text{emit}} \left[(v - \lambda a) S_{-\lambda}(k_i, p_i, k_j) S_{-\lambda}(k_j, p_j, p_{ij}, k_{ij}) \right. \\ &\quad \left. + (v + \lambda a) m_i m_I S_{-\lambda}(k_i, p_j, k_j) S_{-\lambda}(k_j, k_{ij}) \right] \\ M^{f \rightarrow f'V}(\lambda, -\lambda, \lambda) &= A_{\perp}^{\text{emit}} \left[m_I (v + \lambda a) S_{\lambda}(k_i, p_i, k_j) S_{-\lambda}(k_j, p_j, k_{ij}) \right. \\ &\quad \left. - m_i (v - \lambda a) S_{\lambda}(k_i, p_j, k_j) S_{-\lambda}(k_j, p_{ij}, k_{ij}) \right] \\ M^{f \rightarrow f'V}(\lambda, -\lambda, -\lambda) &= A_{\perp}^{\text{emit}} \left[m_I (v + \lambda a) S_{\lambda}(k_i, p_i, p_j, k_j) S_{\lambda}(k_j, k_{ij}) \right. \\ &\quad \left. - m_i (v - \lambda a) S_{\lambda}(k_i, k_j) S_{\lambda}(k_j, p_j, p_{ij}, k_{ij}) \right] \\ M^{f \rightarrow f'V}(\lambda, \lambda, 0) &= A_L^{\text{emit}} \left[S_{-\lambda}(k_i, (v - \lambda a)(m_I^2 p_i - m_i^2 p_j) + (v + \lambda a) m_i m_I p_j, k_{ij}) \right. \\ &\quad \left. - \frac{m_j^2}{p_j \cdot k_j} \left((v - \lambda a) S_{-\lambda}(k_i, p_i, k_j, p_{ij}, k_{ij}) \right. \right. \\ &\quad \left. \left. + (v + \lambda a) m_I m_i S_{-\lambda}(k_i, k_j, k_{ij}) \right) \right] \\ M^{f \rightarrow f'V}(\lambda, -\lambda, 0) &= A_L^{\text{emit}} \left[m_i (v - \lambda a) S_{-\lambda}(k_i, p_j - \frac{m_j^2}{p_j \cdot k_j} k_j, p_{ij}, k_{ij}) \right. \\ &\quad \left. + m_I (v + \lambda a) S_{-\lambda}(k_i, p_i, p_j - \frac{m_j^2}{p_j \cdot k_j} k_j, k_{ij}) \right] \end{aligned}$$

B.1.2 Vector Boson Emission from Antifermion

$$M^{\bar{f} \rightarrow \bar{f}'V}(\lambda, \lambda, \lambda) = A_{\perp}^{\text{emit}} \left[(v + \lambda a) S_{\lambda}(k_{ij}, p_{ij}, k_j) S_{-\lambda}(k_j, p_j, p_i, k_i) \right]$$

$$\begin{aligned}
& + (v - \lambda a) m_i m_I S_\lambda(k_{ij}, p_j, k_j) S_{-\lambda}(k_j, k_i) \Big] \\
M^{\bar{f} \rightarrow \bar{f}' V}(\lambda, \lambda, -\lambda) &= A_\perp^{\text{emit}} \left[(v + \lambda a) S_\lambda(k_{ij}, p_j, k_j) S_{-\lambda}(k_j, p_i, k_i) \right. \\
& \left. + (v - \lambda a) m_i m_I S_\lambda(k_{ij}, k_j) S_{-\lambda}(k_j, p_i, k_i) \right] \\
M^{\bar{f} \rightarrow \bar{f}' V}(\lambda, -\lambda, \lambda) &= A_\perp^{\text{emit}} \left[m_I (v - \lambda a) S_\lambda(k_{ij}, p_j, k_j) S_{-\lambda}(k_j, p_i, k_i) \right. \\
& \left. - m_i (v + \lambda a) S_\lambda(k_{ij}, p_{ij}, k_j) S_{-\lambda}(k_j, p_j, k_i) \right] \\
M^{\bar{f} \rightarrow \bar{f}' V}(\lambda, -\lambda, -\lambda) &= A_\perp^{\text{emit}} \left[m_I (v - \lambda a) S_\lambda(k_{ij}, k_j) S_{-\lambda}(k_j, p_j, p_i, k_i) \right. \\
& \left. - m_i (v + \lambda a) S_\lambda(k_{ij}, p_{ij}, p_j, k_j) S_{-\lambda}(k_j, k_i) \right] \\
M^{\bar{f} \rightarrow \bar{f}' V}(\lambda, \lambda, 0) &= A_L^{\text{emit}} \left[S_\lambda(k_{ij}, (v + \lambda a)(m_I^2 p_i - m_i^2 p_{ij}) + (v - \lambda a) m_I m_i p_j, k_i) \right. \\
& - \frac{m_j^2}{p_j \cdot k_j} \left((v + \lambda a) S_\lambda(k_{ij}, p_{ij}, k_j, p_i, k_i) \right. \\
& \left. \left. + (v - \lambda a) m_I m_i S_\lambda(k_{ij}, k_j, k_i) \right) \right] \\
M^{\bar{f} \rightarrow \bar{f}' V}(\lambda, -\lambda, 0) &= A_L^{\text{emit}} \left[m_i (v + \lambda a) S_\lambda(k_{ij}, p_{ij}, p_j - \frac{m_j^2}{p_j \cdot k_j} k_j, k_i) \right. \\
& \left. + m_I (v - \lambda a) S_\lambda(k_{ij}, p_j - \frac{m_j^2}{p_j \cdot k_j} k_j, p_i, k_i) \right]
\end{aligned}$$

B.1.3 Vector Boson Emission from Vector Boson

The branching amplitude can be written as

$$M^{V \rightarrow V' V''}(\lambda_{ij}, \lambda_i, \lambda_j) = -2g_V (p_j \cdot \epsilon_i \epsilon_j \cdot \bar{\epsilon}_{ij} - p_i \cdot \epsilon_j \epsilon_i \cdot \bar{\epsilon}_{ij} + p_i \cdot \bar{\epsilon}_{ij} \epsilon_i \cdot \epsilon_j) \quad (\text{B.4})$$

To compute the branching amplitude for all helicity configurations, we write out all possible products of momenta and polarization vectors

$$\begin{aligned}
\epsilon_\lambda(p_a) \cdot \epsilon_\lambda(p_b) &= -\frac{1}{4} \frac{1}{p_a \cdot k_a p_b \cdot k_b} S_{-\lambda}(k_a, p_a, p_b, k_b) S_\lambda(k_b, k_a) \\
\epsilon_\lambda(p_a) \cdot \epsilon_{-\lambda}(p_b) &= -\frac{1}{4} \frac{1}{p_a \cdot k_a p_b \cdot k_b} S_\lambda(k_a, p_a, k_b) S_{-\lambda}(k_a, p_b, k_b) \\
\epsilon_\lambda(p_a) \cdot \epsilon_0(p_b) &= \frac{\lambda}{2\sqrt{2}} \frac{1}{m_b} \frac{1}{p_a \cdot k_a} \left(S_{-\lambda}(k_a, p_a, p_b, k_a) - \frac{m_b}{p_b \cdot k_b} S_{-\lambda}(k_a, p_a, k_b, k_a) \right) \\
\epsilon_0(p_a) \cdot \epsilon_0(p_b) &= \frac{1}{m_a m_b} \left(p_a \cdot p_b - \frac{m_a}{p_a \cdot k_a} k_a - \frac{m_b}{p_b \cdot k_b} k_b + \frac{m_a}{p_a \cdot k_a} \frac{m_b}{p_b \cdot k_b} k_a \cdot k_b \right) \\
\epsilon_\lambda(p_a) \cdot p_b &= \frac{\lambda}{\sqrt{2}} \frac{1}{p_a \cdot k_a} S_{-\lambda}(k_a, p_a, p_b, k_a) \\
\epsilon_0(p_a) \cdot p_b &= \frac{1}{m_a} \left(p_a \cdot p_b - \frac{m_a^2}{p_a \cdot k_a} \right)
\end{aligned} \quad (\text{B.5})$$

The unitarity-violating terms are then removed by the substitutions

$$\begin{aligned}
p_i \cdot p_j &\rightarrow \frac{1}{2} (m_I^2 - m_i^2 - m_j^2) \\
p_{ij} \cdot p_i &\rightarrow \frac{1}{2} (m_I^2 + m_i^2 - m_j^2) \\
p_{ij} \cdot p_j &\rightarrow \frac{1}{2} (m_I^2 - m_i^2 + m_j^2)
\end{aligned} \tag{B.6}$$

B.2 Higgs Emission

B.2.1 Higgs Emission from Fermion

$$\begin{aligned}
M^{f \rightarrow fh}(\lambda, -\lambda, h) &= \frac{e}{4s_w} \frac{m_i}{m_w} \frac{1}{\sqrt{p_{ij} \cdot k_{ij}} \sqrt{p_i \cdot k_i}} \left[S_{-\lambda}(k_i, p_i, p_{ij}, k_{ij}) + m_i^2 S_{-\lambda}(k_i, k_{ij}) \right] \\
M^{f \rightarrow fh}(\lambda, \lambda, h) &= \frac{e}{4s_w} \frac{m_i^2}{m_w} \frac{1}{\sqrt{p_{ij} \cdot k_{ij}} \sqrt{p_i \cdot k_i}} S_{-\lambda}(k_i, p_i + p_{ij}, k_{ij})
\end{aligned}$$

B.2.2 Higgs Emission from Antifermion

$$\begin{aligned}
M^{\bar{f} \rightarrow \bar{f}h}(\lambda, -\lambda, h) &= \frac{e}{4s_w} \frac{m_i}{m_w} \frac{1}{\sqrt{p_{ij} \cdot k_{ij}} \sqrt{p_i \cdot k_i}} \left[S_{\lambda}(k_{ij}, p_{ij}, p_i, k_i) + m_i^2 S_{\lambda}(k_{ij}, k_i) \right] \\
M^{\bar{f} \rightarrow \bar{f}h}(\lambda, \lambda, h) &= \frac{e}{4s_w} \frac{m_i^2}{m_w} \frac{1}{\sqrt{p_{ij} \cdot k_{ij}} \sqrt{p_i \cdot k_i}} S_{\lambda}(k_{ij}, p_i + p_{ij}, k_i)
\end{aligned}$$

B.2.3 Higgs Emission from Vector Boson

$$\begin{aligned}
M^{V \rightarrow Vh}(\lambda, \lambda, h) &= -\frac{gh}{4} \frac{1}{p_{ij} \cdot k_{ij} p_i \cdot k_i} S_{-\lambda}(k_{ij}, p_{ij}, k_i) S_{-\lambda}(k_{ij}, p_i, k_i) \\
M^{V \rightarrow Vh}(\lambda, -\lambda, h) &= -\frac{gh}{4} \frac{1}{p_{ij} \cdot k_{ij} p_i \cdot k_i} S_{-\lambda}(k_i, k_{ij}) S_{-\lambda}(k_{ij}, p_{ij}, p_i, k_i) \\
M^{V \rightarrow Vh}(0, \lambda, h) &= -\frac{gh}{2\sqrt{2}} \frac{1}{m_I} \frac{\lambda}{p_i \cdot k_i} S_{-\lambda}(k_i, p_i, p_{ij} - \frac{m_I^2}{p_{ij} \cdot k_{ij}} k_{ij}, k_i) \\
M^{V \rightarrow Vh}(\lambda, 0, h) &= -\frac{gh}{2\sqrt{2}} \frac{1}{m_i} \frac{\lambda}{p_{ij} \cdot k_{ij}} S_{-\lambda}(k_{ij}, p_{ij}, p_i - \frac{m_i^2}{p_i \cdot k_i} k_i, k_{ij}) \\
M^{V \rightarrow Vh}(0, 0, h) &= -\frac{gh}{m_I^2} \left[\frac{1}{2} m_j^2 + m_I^2 \left(\frac{p_i \cdot k_i}{p_{ij} \cdot k_{ij}} + \frac{p_j \cdot k_j}{p_i \cdot k_i} \right) \right]
\end{aligned}$$

B.2.4 Higgs Emission from Higgs

$$M^{h \rightarrow hh}(h, h, h) = \frac{3}{2} \frac{m_I^2}{m_w s_w} \tag{B.7}$$

B.3 Vector Boson Splitting

B.3.1 Vector Boson Splitting to Fermion-antifermion

Defining the prefactors

$$A_{\perp}^{\text{split}} = -\frac{1}{2\sqrt{2}} \frac{\lambda}{p_{ij} \cdot k_{ij} \sqrt{p_i \cdot k_i} \sqrt{p_j \cdot k_j}}$$

$$A_L^{\text{split}} = \frac{1}{2} \frac{1}{m_I} \frac{1}{\sqrt{p_i \cdot k_i} \sqrt{p_j \cdot k_j}} \quad (\text{B.8})$$

the branching amplitudes are

$$\begin{aligned}
M^{V \rightarrow f \bar{f}}(\lambda, \lambda, -\lambda) &= A_{\perp}^{\text{split}} \left[(v - \lambda a) S_{-\lambda}(k_i, p_i, k_{ij}) S_{-\lambda}(k_{ij}, p_{ij}, p_j, k_j) \right. \\
&\quad \left. + (v + \lambda a) m_i m_j S_{-\lambda}(k_i, p_{ij}, k_{ij}) S_{-\lambda}(k_{ij}, k_j) \right] \\
M^{V \rightarrow f \bar{f}}(\lambda, -\lambda, \lambda) &= A_{\perp}^{\text{split}} \left[(v + \lambda a) S_{-\lambda}(k_i, p_i, p_{ij}, k_{ij}) \right. \\
&\quad \left. + (v - \lambda a) m_i m_j S_{-\lambda}(k_i, k_{ij}) S_{-\lambda}(k_{ij}, p_{ij}, k_j) \right] \\
M^{V \rightarrow f \bar{f}}(\lambda, \lambda, \lambda) &= A_{\perp}^{\text{split}} \left[(v + \lambda a) m_i S_{-\lambda}(k_i, p_{ij}, k_{ij}) S_{-\lambda}(k_{ij}, p_j, k_j) \right. \\
&\quad \left. + (v - \lambda a) m_j S_{-\lambda}(k_i, p_i, k_{ij}) S_{-\lambda}(k_{ij}, p_{ij}, k_j) \right] \\
M^{V \rightarrow f \bar{f}}(\lambda, -\lambda, -\lambda) &= A_{\perp}^{\text{split}} \left[(v - \lambda a) m_i S_{-\lambda}(k_i, k_{ij}) S_{-\lambda}(k_{ij}, p_{ij}, p_j, k_j) \right. \\
&\quad \left. + (v + \lambda a) m_j S_{-\lambda}(k_i, p_i, p_{ij}, k_{ij}) S_{-\lambda}(k_{ij}, k_j) \right] \\
M^{V \rightarrow f \bar{f}}(0, \lambda, -\lambda) &= A_L^{\text{split}} \left[S_{-\lambda}(k_i, (v - \lambda a)(m_i^2 p_j + m_j^2 p_i) \right. \\
&\quad \left. - (v + \lambda a) m_i m_j (p_{ij} - \frac{m_I^2}{p_{ij} \cdot k_{ij}}) k_{ij}, k_j) \right. \\
&\quad \left. - \frac{m_I^2}{p_{ij} \cdot k_{ij}} (v - \lambda a) S_{-\lambda}(k_i, p_i, k_{ij}, p_j, k_j) \right] \\
M^{V \rightarrow f \bar{f}}(0, \lambda, \lambda) &= A_L^{\text{split}} \left[m_i (v + \lambda a) S_{-\lambda}(k_i, p_{ij} - \frac{m_I^2}{p_{ij} \cdot k_{ij}} k_{ij}, p_j, k_j) \right. \\
&\quad \left. - m_j (v - \lambda a) S_{-\lambda}(k_i, p_i, p_{ij} - \frac{m_I^2}{p_{ij} \cdot k_{ij}}, k_j) \right]
\end{aligned}$$

B.4 Higgs Splitting

B.4.1 Higgs Splitting to Fermion-antifermion

$$\begin{aligned}
M^{f \rightarrow f h}(\lambda, \lambda, h) &= \frac{e}{4s_w} \frac{m_i}{m_w} \frac{1}{\sqrt{p_i \cdot k_i} \sqrt{p_j \cdot k_j}} \left[S_{-\lambda}(k_i, p_i, p_j, k_j) - m_i^2 S_{-\lambda}(k_i, k_j) \right] \\
M^{f \rightarrow f h}(\lambda, -\lambda, h) &= \frac{e}{4s_w} \frac{m_i^2}{m_w} \frac{1}{\sqrt{p_i \cdot k_i} \sqrt{p_j \cdot k_j}} S_{-\lambda}(k_i, p_i - p_j, k_j)
\end{aligned}$$

B.4.2 Higgs Splitting to Vector Bosons

$$M^{h \rightarrow VV}(h, \lambda, -\lambda) = -\frac{gh}{4} S_{-\lambda}(k_i, p_i, k_j) S_{-\lambda}(k_i, p_j, k_j)$$

$$\begin{aligned}
M^{h \rightarrow VV}(h, \lambda, \lambda) &= -\frac{gh}{4} S_{-\lambda}(k_j, k_i) S_{-\lambda}(k_i, p_i, p_j, k_j) \\
M^{h \rightarrow VV}(h, 0, \lambda) &= -\frac{gh}{2\sqrt{2}} \frac{1}{m_i} \frac{\lambda}{p_j \cdot k_j} S_{-\lambda}(k_j, p_j, p_i - \frac{m_i^2}{p_i \cdot k_i} k_i, k_j) \\
M^{h \rightarrow VV}(h, \lambda, 0) &= -\frac{gh}{2\sqrt{2}} \frac{1}{m_j} \frac{\lambda}{p_i \cdot k_i} S_{-\lambda}(k_i, p_i, p_j - \frac{m_j^2}{p_j \cdot k_k} k_j, k_i) \\
M^{h \rightarrow VV}(h, 0, 0) &= \frac{gh}{m_i m_j} \left[\frac{1}{2} (m_i^2 - m_i^2 - m_j^2) - m_j^2 \frac{p_i \cdot k_i}{p_j \cdot k_j} - m_i^2 \frac{p_j \cdot k_j}{p_i \cdot k_i} \right]
\end{aligned}$$

B.5 Vector Boson Emission (Initial State)

B.5.1 Vector Boson Emission from Fermion

We define the prefactors

$$\begin{aligned}
\tilde{A}_{\perp}^{\text{emit}} &= \frac{1}{2\sqrt{2}} \frac{\lambda}{\sqrt{p_a \cdot k_j} \sqrt{p_{aj} \cdot k_{aj}} p_j \cdot k_j} \\
\tilde{A}_L^{\text{emit}} &= \frac{1}{2} \frac{1}{m_j} \frac{1}{\sqrt{p_a \cdot k_a} \sqrt{p_{aj} \cdot k_{aj}}}.
\end{aligned} \tag{B.9}$$

$$\begin{aligned}
M^{\tilde{f} \rightarrow \tilde{f}' V}(\lambda, \lambda, \lambda) &= \tilde{A}_{\perp}^{\text{emit}} \left[(v - \lambda a) S_{-\lambda}(k_{aj}, p_{aj}, p_j, k_j) S_{-\lambda}(k_j, p_a, k_a) \right. \\
&\quad \left. - (v + \lambda a) m_a m_A S_{-\lambda}(k_{aj}, k_j) S_{-\lambda}(k_j, p_j, k_a) \right] \\
M^{\tilde{f} \rightarrow \tilde{f}' V}(\lambda, \lambda, -\lambda) &= \tilde{A}_{\perp}^{\text{emit}} \left[(v - \lambda a) S_{-\lambda}(k_{aj}, p_{aj}, k_j) S_{-\lambda}(k_j, p_j, p_a, k_a) \right. \\
&\quad \left. - (v + \lambda a) m_a m_A S_{-\lambda}(k_{aj}, p_j, k_j) S_{-\lambda}(k_j, k_a) \right] \\
M^{\tilde{f} \rightarrow \tilde{f}' V}(\lambda, -\lambda, \lambda) &= \tilde{A}_{\perp}^{\text{emit}} \left[(v + \lambda a) m_A S_{-\lambda}(k_{aj}, k_j) S_{-\lambda}(k_j, p_j, p_a, k_a) \right. \\
&\quad \left. - (v - \lambda a) m_a S_{-\lambda}(k_{aj}, p_{aj}, p_j, k_j) S_{-\lambda}(k_j, k_a) \right] \\
M^{\tilde{f} \rightarrow \tilde{f}' V}(\lambda, -\lambda, -\lambda) &= \tilde{A}_{\perp}^{\text{emit}} \left[(v + \lambda a) m_A S_{-\lambda}(k_{aj}, p_j, k_j) S_{-\lambda}(k_j, p_a, k_a) \right. \\
&\quad \left. - (v - \lambda a) m_a S_{-\lambda}(k_{aj}, p_{aj}, k_j) S_{-\lambda}(k_j, p_j, k_a) \right] \\
M^{\tilde{f} \rightarrow \tilde{f}' V}(\lambda, \lambda, 0) &= \tilde{A}_L^{\text{emit}} \left[S_{-\lambda}(k_{aj}, (v - \lambda a)(m_a^2 p_{aj} - m_A^2 p_a) + (v + \lambda a) m_a m_A p_j, k_a) \right. \\
&\quad \left. - \frac{m_j^2}{p_j \cdot k_j} \left((v - \lambda a) S_{-\lambda}(k_{aj}, p_{aj}, k_j, p_a, k_a) \right. \right. \\
&\quad \left. \left. - (v + \lambda a) m_A m_a S_{-\lambda}(k_{aj}, k_j, k_a) \right) \right] \\
M^{\tilde{f} \rightarrow \tilde{f}' V}(\lambda, -\lambda, 0) &= \tilde{A}_L^{\text{emit}} \left[m_A (v - \lambda a) S_{-\lambda}(k_{aj}, p_j - \frac{m_j^2}{p_j \cdot k_j} k_j, p_a, k_a) \right.
\end{aligned}$$

$$+ m_A(v + \lambda a)S_{-\lambda}(k_{aj}, p_{aj}, p_j - \frac{m_j^2}{p_j \cdot k_j} k_j, k_a) \Big]$$

B.5.2 Vector Boson Emission from Antifermion

$$M^{\tilde{f} \rightarrow \tilde{f}' V}(\lambda, \lambda, \lambda) = \tilde{A}_{\perp}^{\text{emit}} \left[(v + \lambda a)S_{\lambda}(k_a, p_a, k_j)S_{-\lambda}(k_j, p_j p_{aj}, k_{aj}) \right. \\ \left. - (v - \lambda a)m_a m_A S_{\lambda}(k_a, p_j, k_j)S_{-\lambda}(k_j, k_{aj}) \right]$$

$$M^{\tilde{f} \rightarrow \tilde{f}' V}(\lambda, \lambda, -\lambda) = \tilde{A}_{\perp}^{\text{emit}} \left[(v + \lambda a)S_{\lambda}(k_a, p_a, p_j, k_j)S_{-\lambda}(k_j, p_{aj}, k_{aj}) \right. \\ \left. - (v - \lambda a)m_a m_A S_{\lambda}(k_a, k_j)S_{-\lambda}(k_j, p_j, k_a) \right]$$

$$M^{\tilde{f} \rightarrow \tilde{f}' V}(\lambda, -\lambda, \lambda) = \tilde{A}_{\perp}^{\text{emit}} \left[(v - \lambda a)m_a S_{\lambda}(k_a, p_j, k_j)S_{-\lambda}(k_j, p_{aj}, k_{aj}) \right. \\ \left. - (v + \lambda a)m_A S_{\lambda}(k_a, p_a, k_j)S_{-\lambda}(k_j, p_j, k_{aj}) \right]$$

$$M^{\tilde{f} \rightarrow \tilde{f}' V}(\lambda, -\lambda, -\lambda) = \tilde{A}_{\perp}^{\text{emit}} \left[(v - \lambda a)m_a S_{\lambda}(k_a, k_j)S_{-\lambda}(k_j, p_j, p_{aj}, k_{aj}) \right. \\ \left. - (v + \lambda a)m_A S_{\lambda}(k_a, p_a, p_j, k_j)S_{-\lambda}(k_j, k_{aj}) \right]$$

$$M^{\tilde{f} \rightarrow \tilde{f}' V}(\lambda, \lambda, 0) = \tilde{A}_L^{\text{emit}} \left[S_{\lambda}(k_a, (v + \lambda a)(m_a^2 p_{aj} - m_A^2 p_a) + (v - \lambda a)m_a m_A p_j, k_{aj}) \right. \\ \left. - \frac{m_j^2}{p_j \cdot k_j} \left((v + \lambda a)S_{\lambda}(k_a, p_a, k_j, p_{aj}, k_{aj}) \right. \right. \\ \left. \left. - (v - \lambda a)m_A m_a S_{\lambda}(k_a, k_j, k_{aj}) \right) \right]$$

$$M^{\tilde{f} \rightarrow \tilde{f}' V}(\lambda, -\lambda, 0) = \tilde{A}_L^{\text{emit}} \left[m_a(v - \lambda a)S_{\lambda}(k_a, p_j - \frac{m_j^2}{p_j \cdot k_j} k_j, p_{aj}, k_{aj}) \right. \\ \left. + m_A(v + \lambda a)S_{\lambda}(k_a, p_a, p_j - \frac{m_j^2}{p_j \cdot k_j} k_j, k_{aj}) \right]$$

References

- [1] ATLAS collaboration, *Observation of a new particle in the search for the Standard Model Higgs boson with the ATLAS detector at the LHC*, *Phys. Lett.* **B716** (2012) 1 [1207.7214].
- [2] CMS collaboration, *Observation of a new boson at a mass of 125 GeV with the CMS experiment at the LHC*, *Phys. Lett.* **B716** (2012) 30 [1207.7235].
- [3] S. Dawson, A. Ismail and I. Low, *Redux on “When is the top quark a parton?”*, *Phys. Rev.* **D90** (2014) 014005 [1405.6211].
- [4] L. G. Almeida, S. J. Lee, G. Perez, I. Sung and J. Virzi, *Top Jets at the LHC*, *Phys. Rev.* **D79** (2009) 074012 [0810.0934].
- [5] W. Beenakker, A. Denner, S. Dittmaier, R. Mertig and T. Sack, *High-energy approximation for on-shell W pair production*, *Nucl. Phys.* **B410** (1993) 245.

- [6] W. Beenakker, A. Denner, S. Dittmaier and R. Mertig, *On shell W pair production in the TeV range*, *Phys. Lett.* **B317** (1993) 622.
- [7] W. Beenakker, A. Denner, W. Hollik, R. Mertig, T. Sack and D. Wackerroth, *Electroweak one loop contributions to top pair production in hadron colliders*, *Nucl. Phys.* **B411** (1994) 343.
- [8] V. S. Fadin, L. N. Lipatov, A. D. Martin and M. Melles, *Resummation of double logarithms in electroweak high-energy processes*, *Phys. Rev.* **D61** (2000) 094002 [[hep-ph/9910338](#)].
- [9] J. H. Kuhn, A. A. Penin and V. A. Smirnov, *Summing up subleading Sudakov logarithms*, *Eur. Phys. J.* **C17** (2000) 97 [[hep-ph/9912503](#)].
- [10] M. Ciafaloni, P. Ciafaloni and D. Comelli, *Bloch-Nordsieck violating electroweak corrections to inclusive TeV scale hard processes*, *Phys. Rev. Lett.* **84** (2000) 4810 [[hep-ph/0001142](#)].
- [11] A. Denner and S. Pozzorini, *One loop leading logarithms in electroweak radiative corrections. 1. Results*, *Eur. Phys. J.* **C18** (2001) 461 [[hep-ph/0010201](#)].
- [12] A. Denner and S. Pozzorini, *One loop leading logarithms in electroweak radiative corrections. 2. Factorization of collinear singularities*, *Eur. Phys. J.* **C21** (2001) 63 [[hep-ph/0104127](#)].
- [13] M. Melles, *Resummation of angular dependent corrections in spontaneously broken gauge theories*, *Eur. Phys. J.* **C24** (2002) 193 [[hep-ph/0108221](#)].
- [14] S. Moretti, M. R. Nolten and D. A. Ross, *Weak corrections to four-parton processes*, *Nucl. Phys.* **B759** (2006) 50 [[hep-ph/0606201](#)].
- [15] S. Dittmaier, A. Huss and C. Speckner, *Weak radiative corrections to dijet production at hadron colliders*, *JHEP* **11** (2012) 095 [[1210.0438](#)].
- [16] T. Becher and X. Garcia i Tormo, *Electroweak Sudakov effects in W, Z and γ production at large transverse momentum*, *Phys. Rev.* **D88** (2013) 013009 [[1305.4202](#)].
- [17] J. H. Kuhn, A. Kulesza, S. Pozzorini and M. Schulze, *Electroweak corrections to hadronic production of W bosons at large transverse momenta*, *Nucl. Phys.* **B797** (2008) 27 [[0708.0476](#)].
- [18] W. Hollik, T. Kasprzik and B. A. Kniehl, *Electroweak corrections to W-boson hadroproduction at finite transverse momentum*, *Nucl. Phys.* **B790** (2008) 138 [[0707.2553](#)].
- [19] M. L. Mangano et al., *Physics at a 100 TeV pp Collider: Standard Model Processes*, *CERN Yellow Rep.* (2017) 1 [[1607.01831](#)].
- [20] T. Golling et al., *Physics at a 100 TeV pp collider: beyond the Standard Model phenomena*, *CERN Yellow Rep.* (2017) 441 [[1606.00947](#)].
- [21] ATLAS collaboration, *Measurement of W boson angular distributions in events with high transverse momentum jets at $\sqrt{s} = 8$ TeV using the ATLAS detector*, *Phys. Lett.* **B765** (2017) 132 [[1609.07045](#)].
- [22] J. R. Christiansen and T. Sjöstrand, *Weak Gauge Boson Radiation in Parton Showers*, *JHEP* **04** (2014) 115 [[1401.5238](#)].
- [23] J. R. Christiansen and S. Prestel, *Merging weak and QCD showers with matrix elements*, *Eur. Phys. J.* **C76** (2016) 39 [[1510.01517](#)].
- [24] T. Sjöstrand, S. Ask, J. R. Christiansen, R. Corke, N. Desai, P. Ilten et al., *An Introduction to PYTHIA 8.2*, *Comput. Phys. Commun.* **191** (2015) 159 [[1410.3012](#)].

- [25] T. Gleisberg, S. Höche, F. Krauss, M. Schonherr, S. Schumann, F. Siegert et al., *Event generation with SHERPA 1.1*, *JHEP* **02** (2009) 007 [[0811.4622](#)].
- [26] F. Krauss, P. Petrov, M. Schoenherr and M. Spannowsky, *Measuring collinear W emissions inside jets*, *Phys. Rev.* **D89** (2014) 114006 [[1403.4788](#)].
- [27] M. Chiesa, G. Montagna, L. Barzè, M. Moretti, O. Nicosini, F. Piccinini et al., *Electroweak Sudakov Corrections to New Physics Searches at the LHC*, *Phys. Rev. Lett.* **111** (2013) 121801 [[1305.6837](#)].
- [28] M. L. Mangano, M. Moretti, F. Piccinini, R. Pittau and A. D. Polosa, *ALPGEN, a generator for hard multiparton processes in hadronic collisions*, *JHEP* **07** (2003) 001 [[hep-ph/0206293](#)].
- [29] J. Chen, T. Han and B. Tweedie, *Electroweak Splitting Functions and High Energy Showering*, *JHEP* **11** (2017) 093 [[1611.00788](#)].
- [30] W. T. Giele, D. A. Kosower and P. Z. Skands, *A simple shower and matching algorithm*, *Phys. Rev.* **D78** (2008) 014026 [[0707.3652](#)].
- [31] W. T. Giele, D. A. Kosower and P. Z. Skands, *Higher-Order Corrections to Timelike Jets*, *Phys. Rev.* **D84** (2011) 054003 [[1102.2126](#)].
- [32] M. Ritzmann, D. A. Kosower and P. Skands, *Antenna Showers with Hadronic Initial States*, *Phys. Lett.* **B718** (2013) 1345 [[1210.6345](#)].
- [33] A. J. Larkoski, J. J. Lopez-Villarejo and P. Skands, *Helicity-Dependent Showers and Matching with VINCIA*, *Phys. Rev.* **D87** (2013) 054033 [[1301.0933](#)].
- [34] N. Fischer, A. Lifson and P. Skands, *Helicity Antenna Showers for Hadron Colliders*, *Eur. Phys. J.* **C77** (2017) 719 [[1708.01736](#)].
- [35] A. J. Larkoski and M. E. Peskin, *Spin-Dependent Antenna Splitting Functions*, *Phys. Rev.* **D81** (2010) 054010 [[0908.2450](#)].
- [36] A. J. Larkoski and M. E. Peskin, *Antenna Splitting Functions for Massive Particles*, *Phys. Rev.* **D84** (2011) 034034 [[1106.2182](#)].
- [37] G. Altarelli and G. Parisi, *Asymptotic Freedom in Parton Language*, *Nucl. Phys.* **B126** (1977) 298.
- [38] R. Kleiss and W. J. Stirling, *Spinor Techniques for Calculating p anti- $p \rightarrow W^\pm / Z_0 + Jets$* , *Nucl. Phys.* **B262** (1985) 235.
- [39] G. Abeloﬀ and A. Gehrmann-De Ridder, *Antenna subtraction for the production of heavy particles at hadron colliders*, *JHEP* **04** (2011) 063 [[1102.2443](#)].
- [40] S. Catani, S. Dittmaier and Z. Trocsanyi, *One loop singular behavior of QCD and SUSY QCD amplitudes with massive partons*, *Phys. Lett.* **B500** (2001) 149 [[hep-ph/0011222](#)].
- [41] V. N. Gribov and L. N. Lipatov, *Deep inelastic $e p$ scattering in perturbation theory*, *Sov. J. Nucl. Phys.* **15** (1972) 438.
- [42] Y. L. Dokshitzer, *Calculation of the Structure Functions for Deep Inelastic Scattering and $e^+ e^-$ Annihilation by Perturbation Theory in Quantum Chromodynamics.*, *Sov. Phys. JETP* **46** (1977) 641.
- [43] R. K. Ellis, W. J. Stirling and B. R. Webber, *QCD and collider physics*, *Camb. Monogr. Part. Phys. Nucl. Phys. Cosmol.* **8** (1996) 1.

- [44] S. Platzer and S. Gieseke, *Coherent Parton Showers with Local Recoils*, *JHEP* **01** (2011) 024 [[0909.5593](#)].
- [45] S. Schumann and F. Krauss, *A Parton shower algorithm based on Catani-Seymour dipole factorisation*, *JHEP* **03** (2008) 038 [[0709.1027](#)].
- [46] L. Lonnblad, *ARIADNE version 4: A Program for simulation of QCD cascades implementing the color dipole model*, *Comput. Phys. Commun.* **71** (1992) 15.
- [47] S. Höche and S. Prestel, *The midpoint between dipole and parton showers*, *Eur. Phys. J.* **C75** (2015) 461 [[1506.05057](#)].
- [48] R. Kleiss and R. Verheyen, *Final-state QED Multipole Radiation in Antenna Parton Showers*, *JHEP* **11** (2017) 182 [[1709.04485](#)].
- [49] P. Skands and R. Verheyen, *Multipole Photon Radiation in the Vincia Parton Shower*, [2002.04939](#).
- [50] A. Gehrmann-De Ridder, M. Ritzmann and P. Z. Skands, *Timelike Dipole-Antenna Showers with Massive Fermions*, *Phys. Rev.* **D85** (2012) 014013 [[1108.6172](#)].
- [51] N. Fischer, S. Prestel, M. Ritzmann and P. Skands, *Vincia for Hadron Colliders*, *Eur. Phys. J.* **C76** (2016) 589 [[1605.06142](#)].
- [52] H. Brooks and P. Skands, *Coherent Showers in Decays of Coloured Resonances*, [1907.08980](#).
- [53] M. Bahr et al., *Herwig++ Physics and Manual*, *Eur. Phys. J.* **C58** (2008) 639 [[0803.0883](#)].
- [54] J. Bellm et al., *Herwig 7.2 Release Note*, [1912.06509](#).
- [55] P. Richardson and S. Webster, *Spin Correlations in Parton Shower Simulations*, [1807.01955](#).
- [56] Z. Nagy and D. E. Soper, *Parton showers with quantum interference: Leading color, spin averaged*, *JHEP* **03** (2008) 030 [[0801.1917](#)].
- [57] Z. Nagy and D. E. Soper, *Parton showers with quantum interference: Leading color, with spin*, *JHEP* **07** (2008) 025 [[0805.0216](#)].
- [58] J. R. Forshaw, J. Holguin and S. Plätzer, *Parton branching at amplitude level*, [1905.08686](#).
- [59] Z. Nagy and D. E. Soper, *Parton showers with more exact color evolution*, *Phys. Rev.* **D99** (2019) 054009 [[1902.02105](#)].
- [60] S. Plätzer, M. Sjö Dahl and J. Thorén, *Color matrix element corrections for parton showers*, *JHEP* **11** (2018) 009 [[1808.00332](#)].
- [61] J. Isaacson and S. Prestel, *Stochastically sampling color configurations*, *Phys. Rev.* **D99** (2019) 014021 [[1806.10102](#)].
- [62] T. Sjöstrand, S. Mrenna and P. Z. Skands, *PYTHIA 6.4 Physics and Manual*, *JHEP* **05** (2006) 026 [[hep-ph/0603175](#)].
- [63] H. Brooks, P. Skands and R. Verheyen, *Upcoming publication*, .
- [64] P. Ciafaloni and D. Comelli, *Electroweak evolution equations*, *JHEP* **11** (2005) 022 [[hep-ph/0505047](#)].
- [65] L. Lonnblad, *Fooling Around with the Sudakov Veto Algorithm*, *Eur. Phys. J.* **C73** (2013) 2350 [[1211.7204](#)].
- [66] S. Platzer and M. Sjö Dahl, *The Sudakov Veto Algorithm Reloaded*, *Eur. Phys. J. Plus* **127** (2012) 26 [[1108.6180](#)].

- [67] R. Kleiss and R. Verheyen, *Competing Sudakov Veto Algorithms*, *Eur. Phys. J.* **C76** (2016) 359 [[1605.09246](#)].
- [68] G. Rossum, *Python reference manual*, tech. rep., Amsterdam, The Netherlands, The Netherlands, 1995.
- [69] J. Roy and S. A. Mitchell, “Pulp.” <https://pythonhosted.org/PuLP/>.
- [70] R. D. Ball et al., *Parton distributions with LHC data*, *Nucl. Phys.* **B867** (2013) 244 [[1207.1303](#)].
- [71] N. Cabibbo, *Unitary Symmetry and Leptonic Decays*, *Phys. Rev. Lett.* **10** (1963) 531.
- [72] M. Kobayashi and T. Maskawa, *CP Violation in the Renormalizable Theory of Weak Interaction*, *Prog. Theor. Phys.* **49** (1973) 652.
- [73] M. Ciafaloni, P. Ciafaloni and D. Comelli, *Electroweak Bloch-Nordsieck violation at the TeV scale: ‘Strong’ weak interactions?*, *Nucl. Phys.* **B589** (2000) 359 [[hep-ph/0004071](#)].
- [74] S. Dawson, *The Effective W Approximation*, *Nucl. Phys.* **B249** (1985) 42.
- [75] G. L. Kane, W. W. Repko and W. B. Rolnick, *The Effective W^{+-} , $Z0$ Approximation for High-Energy Collisions*, *Phys. Lett.* **148B** (1984) 367.
- [76] S. Carrazza, *Parton distribution functions with QED corrections*, Ph.D. thesis, Milan U., 2015. [1509.00209](#).
- [77] C. Schmidt, J. Pumplin, D. Stump and C. P. Yuan, *CT14QED parton distribution functions from isolated photon production in deep inelastic scattering*, *Phys. Rev.* **D93** (2016) 114015 [[1509.02905](#)].
- [78] A. Manohar, P. Nason, G. P. Salam and G. Zanderighi, *How bright is the proton? A precise determination of the photon parton distribution function*, *Phys. Rev. Lett.* **117** (2016) 242002 [[1607.04266](#)].
- [79] C. W. Bauer, N. Ferland and B. R. Webber, *Standard Model Parton Distributions at Very High Energies*, *JHEP* **08** (2017) 036 [[1703.08562](#)].
- [80] C. W. Bauer, N. Ferland and B. R. Webber, *Combining initial-state resummation with fixed-order calculations of electroweak corrections*, *JHEP* **04** (2018) 125 [[1712.07147](#)].
- [81] C. W. Bauer and B. R. Webber, *Polarization Effects in Standard Model Parton Distributions at Very High Energies*, *JHEP* **03** (2019) 013 [[1808.08831](#)].